Contents

I. Materials and Methods

1. General Experimental Methods

All reagents and solvents were of commercial reagent grade and were used without further purification except where noted. Silica gel column chromatography was performed on Wakogel® C-200 and C-300. Alumina column chromatography was performed on Sumitomo Active alumina. Thin-layer chromatography (TLC) was carried out on aluminum sheets coated with silica gel 60 F_{254} (Merck 5554). ^{1}H (600.17 MHz) and ^{19}F (564.73 MHz) NMR spectra were recorded on a JEOL ECA-600 spectrometer, and chemical shifts were reported as the delta scale in ppm relative to $CHCl_3$ as internal reference for ^{1}H (δ = 7.260 ppm), and hexafluorobenzene as external reference for ^{19}F (δ = –162.9 ppm). NMR signals were assigned from the ^{1}H–^{1}H COSY spectra and comparison with the spectra in the presence of D_2O (signals assigned for NH protons disappear in the presence of D_2O). High-resolution ESI-TOF mass spectra of samples in acetonitrile were recorded on a BRUKER micrOTOF LC by using the ESI-TOF method in the positive and negative ion mode. UV/Vis/NIR absorption spectra were recorded on a Shimadzu UV-3600PC spectrometer. X-Ray single crystal diffraction analyses were performed on a Rigaku XtaLAB P200 apparatus at –180 °C using two-dimensional detector PILATUS 100K/R with CuKα radiation (λ = 1.54187 Å). The structures were solved by direct method SIR-97 and refined by SHELXL-97 program.

2. Synthetic Procedures and Compound Data

5,20-bis(α-bithienyl)-10,15,25,30-tetrakis(pentafluorophenyl) [26]hexaphyrins T2 and 5,20-bis (α-terthienyl)-10,15,25,30-tetrakis(pentafluorophenyl) [26]hexaphyrins T3.

To a solution of 5,10-bis(pentafluorophenyl)tripyrromethane (280 mg, 0.50 mmol; 1.0 equiv) and the corresponding oligothiophene-5-carbaldehyde (1.0 equiv) in dry dichloromethane (10.0 mM) was added methanesulfonic acid (2.5 M diluted with CH_2Cl_2; 20 mol%), and the resulting solution was stirred under N_2 atmosphere at 0 °C for 2 h. After the addition of 2,3-dichloro-5,6-dicyanobenzoquinone (DDQ; 5.0 equiv), the solution was stirred for another 15 min, and then passed through a short alumina column with CH_2Cl_2 to remove tar. The reaction mixture was purified by silica-gel chromatography (CH_2Cl_2 : *n*-hexane = 1:2) followed by recrystallization from CH_2Cl_2/*n*-hexane to give the corresponding hexaphyrins. **T2** as black crystals (85 mg; 22% yield) and **T3** as brown crystals (43 mg; 10% yield), respectively.

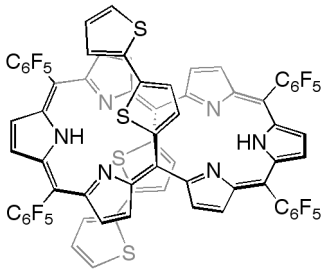

T2: ^{1}H NMR (600 MHz, $CDCl_3$, 213 K): δ (ppm) 8.23 (br s, 1H; inner NH), 8.21 (d, 2H, J = 3.7 Hz; outer β-H), 8.16 (s, 2H; outer β-H), 7.89 (d, 2H, J = 3.7 Hz; outer β-H), 7.70 (d, 2H, J = 4.0 Hz; outer β-H), 7.61 (s, 2H; outer β-H), 6.88 (d, 2H, J = 3.7 Hz; bithienyl-H), 6.34 (t, 2H, J = 3.7 Hz; bithienyl-H), 5.76 (d, 2H, J = 4.0 Hz; outer β-H), 5.28 (d, 2H, J = 4.6 Hz; bithienyl-H), 5.13 (s, 2H, bithienyl-H), 5.12 (br s, 1H; inner NH), and 4.72 (d, 2H, J = 4.6 Hz; bithienyl-H); ^{19}F NMR (565 MHz, $CDCl_3$, 213 K): δ (ppm) –136.34 (d, 2F, J = 23.0 Hz; *o*-F), –136.52 (d, 2F, J = 23.0 Hz; *o*-F), –136.87 (d, 2F, J = 23.0 Hz; *o*-F), –138.03 (d, 2F, J = 23.0 Hz; *o*-F), –150.11 (t, 2F, J = 22.0 Hz; *p*-F), –150.51 (t, 2F, J = 22.0 Hz; *p*-F), –159.36 (br s, 2F; *m*-F), –159.60 (br s, 2F; *m*-F), –159.80 (br s, 2F; *m*-F), and –161.08 (br s, 2F; *m*-F). UV/vis (in CH_2Cl_2): λ_{max}[nm] (ε [$M^{-1}cm^{-1}$]) = 380 (80000), 484 (36000), 548 (41000), 636 (40000), 950 (11000), 1080 (7000).

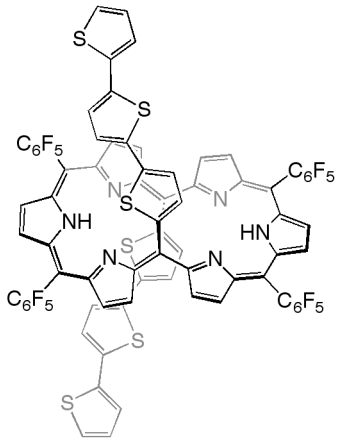

T3: ^{1}H NMR (600 MHz, $CDCl_3$, 213 K): δ (ppm) 8.35 (br s, 1H; inner NH), 8.20 (d, 2H, J = 4.1 Hz; outer β-H), 8.16 (s, 2H; outer β-H), 7.87 (d, 2H, J = 4.1 Hz; outer β-H), 7.76 (d, 2H, J = 4.6 Hz; outer β-H), 7.60 (s, 2H; outer β-H), 7.20 (d, 2H, J = 4.6 Hz; terthienyl-H), 6.97 (m, 2H; terthienyl-H), 6.90 (d, 2H, J = 3.2 Hz; terthienyl-H), 6.45 (d, 2H, J = 3.2 Hz; terthienyl-H), 5.98 (d, 2H, J = 4.6 Hz; outer β-H), 5.29 (d, 2H, J = 4.1 Hz; terthienyl-H), 5.22 (br s, 1H; inner NH), 5.15 (br s, 2H; terthienyl-H), and 4.78 (d, 2H, J = 4.1 Hz; terthienyl-H); ^{19}F NMR (565 MHz, $CDCl_3$, 213 K): δ (ppm) –136.41 (d, 2F, J = 23.0 Hz; *o*-F), –136.58 (d, 2F, J = 23.0 Hz; *o*-F), –136.87 (d, 2F, J = 23.0 Hz; *o*-F), –137.96 (d, 2F, J = 23.0 Hz; *o*-F), –150.11 (t, 2F, J = 22.0 Hz; *p*-F), –150.82 (t, 2F, J = 22.0 Hz; *p*-F), –159.35 (m, 4F; *m*-F), –159.79 (br s, 2F; *m*-F), and –160.95 (br s, 2F; *m*-F). UV/vis (in CH_2Cl_2): λ_{max}[nm] (ε [$M^{-1}cm^{-1}$]) = 418 (95000), 650 (37000), and 975 (10000).

α-quaterthiophene-5-carbaldehyde s3

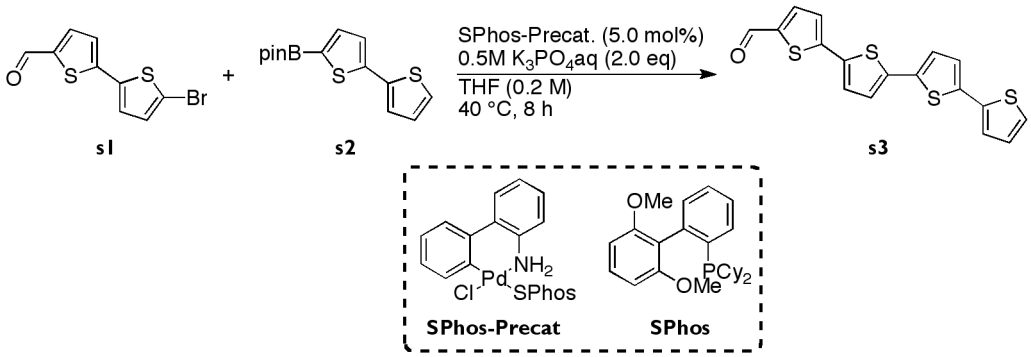

According to the literature,[S1, S2] **s1** (273 mg, 1.0 mmol), **s2** (440 mg, 1.5 mmol), **SPhos-Precat.** (36 mg, 5 mol%), and dry THF (5.0 mL; 0.2 M) were added to a Schlenk tube. To the mixture, degassed 0.5 M K_3PO_4 aq. (4.0 mL, 2.0 mmol) was added. The reaction mixture was stirred at 40 °C. After 8 h, the mixture was cooled to room temperature and CH_2Cl_2 was added to dissolve the solids. The organic phase was dried over Na_2SO_4. The solvent was removed under reduced pressure and the residue was purified by silica gel column chromatography (CH_2Cl_2) and recrystallization with CH_2Cl_2/MeOH to give **s3** as brown solids (270 mg, 75% yield).

[S1] T. Kinzel, Y. Zhang, S. L. Buchwald, *J. Am. Chem. Soc.* 2010, **132**, 14073.

[S2] N. C. Bruno, M. T. Tudge, S. L. Buchwald, *Chem. Sci.* 2013, **4**, 916.

s3: ^{1}H NMR (600 MHz, $CDCl_3$, 300 K): δ (ppm) 9.87 (s, 1H), 7.67 (d, 1H, J = 3.7 Hz), 7.28 (d, 1H, J = 3.7 Hz), 7.25 (m, 2H), 7.20 (dd, 1H, J_1 = 0.9 Hz, J_2 = 3.7 Hz), 7.13 (m, 2H), 7.10 (d, 1H, J = 3.7 Hz), and 7.04 (dd, 1H, J_1 = 3.7 Hz, J_2 = 5.0 Hz); ^{13}C NMR (151 MHz, $CDCl_3$, 300 K): δ (ppm) 182.53, 141.83, 139.01, 137.51, 137.48, 136.93, 135.20, 134.68, 128.14, 127.13, 125.27, 125,07, 124.70, 124.64, and 124.22.

5,20-bis(α-quaterthienyl)-10,15,25,30-tetrakis(pentafluorophenyl) [26]hexaphyrins T4

To a solution of 5,10-bis(pentafluorophenyl)tripyrromethane (140 mg, 0.25 mmol; 1.0 equiv) and α-quaterthiophene-5-carbaldehyde **s3** (90 mg; 1.0 equiv) in dry dichloromethane (25 ml; 10.0 mM) was added methanesulfonic acid (2.5 M diluted with CH_2Cl_2; 20 mol%), and the resulting solution was stirred under N_2 atmosphere at 0 °C for 2 h. After the addition of 2,3-dichloro-5,6-dicyanobenzoquinone (284 mg; 5.0 equiv), the solution was stirred for another 20 min, and then passed through a short alumina column with CH_2Cl_2 as an eluent. The reaction mixture was purified by silica-gel chromatography (CH_2Cl_2 : *n*-hexane = 1:1) followed by recrystallization from CH_2Cl_2/*n*-hexane to give **T4** as greenish crystals (34 mg, 15%).

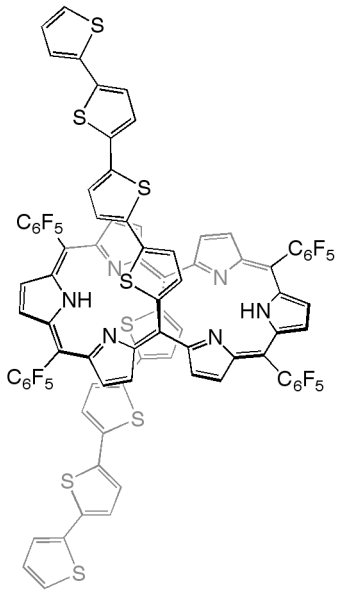

T4: ^{1}H NMR (600 MHz, $CDCl_3$, 213 K): δ (ppm) 8.41 (br s, 1H; inner NH), 8.19 (d, 2H, J = 4.1 Hz; outer β-H), 8.14 (s, 2H; outer β-H), 7.86 (d, 2H, J = 4.1 Hz; outer β-H), 7.79 (d, 2H, J = 4.6 Hz; outer β-H), 7.59 (s, 2H; outer β-H), 7.25 (dd, 2H, J_1 = 0.9 Hz, J_2 = 5.0 Hz; quaterthienyl-H), 7.15 (dd, 2H, J_1 = 0.9 Hz, J_2 = 5.0 Hz; quaterthienyl-H), 7.02 (m, 2H; quaterthienyl-H), 7.01 (d, 2H, J = 3.7 Hz; quaterthienyl-H), 6.81 (d, 2H, J = 3.7 Hz; quaterthienyl-H), 6.45 (d, 2H, J = 3.6 Hz; quaterthienyl-H), 6.05 (d, 2H, J = 4.6 Hz; outer β-H), 5.41 (br s, 1H; inner NH), 5.30 (d, 2H, J = 4.1 Hz; quaterthienyl-H), 5.20 (d, 2H, J = 3.6 Hz; quaterthienyl-H), and 4.82 (d, 2H, J = 4.1 Hz; quaterthienyl-H); ^{19}F NMR (565 MHz, $CDCl_3$, 213 K): δ (ppm) –136.53 (m, 4F; *o*-F), –136.90 (d, 2F, J = 23.0 Hz; *o*-F), –138.00 (d, 2F, J = 23.0 Hz; *o*-F), –150.34 (t, 2F, J = 22.0 Hz; *p*-F), –150.88 (t, 2F, J = 22.0 Hz;

p-F), –159.60 (m, 4F; *m*-F), –160.02 (br s, 2F; *m*-F), and –161.00 (br s, 2F; *m*-F). UV / vis (in CH_2Cl_2): λ_{max}[nm] (ε [$M^{-1}cm^{-1}$]) = 432 (102000), 557 (60000), and 1004 (17000).

5,15-bis(pentafluorophenyl)-10,20-bis(2-thienyl)porphyrin P1 &

5,15-bis(pentafluorophenyl)-10,20-bis(5-bromo-2-thienyl)porphyrin P1Br

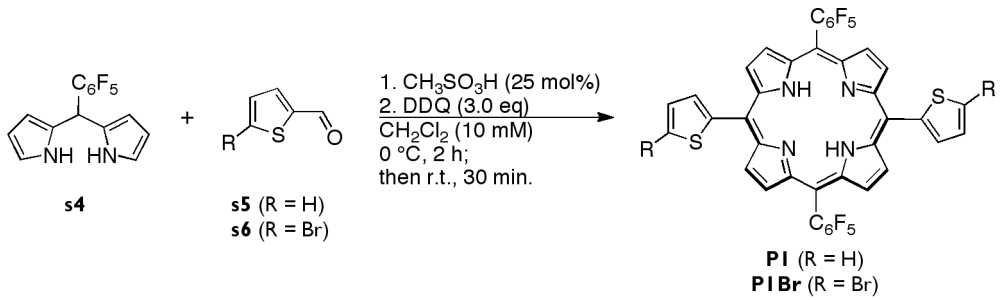

To a solution of 5-pentafluorophenyldipyrromethane **s4** (156 mg, 0.50 mmol; 1.0 equiv) and the corresponding thiophene-carboxaldehyde **s5** or **s6** (1.0 equiv) in dry dichloromethane (50 ml; 10 mM) was added methanesulfonic acid (2.5 M diluted with CH_2Cl_2; 25 mol%), and the resulting solution was stirred under N_2 atmosphere at 0 °C for 2 h. After the addition of 2,3-dichloro-5,6-dicyanobenzoquinone (340 mg; 3.0 equiv), the solution was stirred for another 30 min, and then passed through a short alumina column with CH_2Cl_2 as an eluent. The reaction mixture was purified by silica-gel chromatography (CH_2Cl_2 : *n*-hexane = 1:1) followed by recrystallization from CH_2Cl_2 / *n*-hexane to give **P1** (65 mg, 32%) or **P1Br** (156 mg, 56%) as purple crystals.

P1: ^{1}H NMR (600 MHz, $CDCl_3$, 300 K): δ (ppm) 9.15 (d, 4H, J = 4.6 Hz; β-H), 8.79 (d, 4H, J = 4.6 Hz; β-H), 7.95 (dd, 2H, J_1 = 5.5 Hz, J_2 = 1.4 Hz; thienyl-H), 7.90 (br d, 2H, J = 5.5 Hz; thienyl-H), 7.53 (dd, 2H, J_1 = 5.5 Hz, J_2 = 3.2 Hz; thienyl-H), and –2.74 (br s, 2H; inner NH); ^{19}F NMR (565 MHz, $CDCl_3$, 300 K): δ (ppm) –136.66 (dd, 4F, J_1 = 25.2 Hz, J_2 = 7.0 Hz; *o*-F), –152.11 (t, 2F, J = 22.0 Hz; *p*-F), and –160.90 (br t, 4H, J = 22.0 Hz; *m*-F). UV / vis (in CH_2Cl_2): λ_{max}[nm] (ε [$M^{-1}cm^{-1}$]) = = 419 (360000), 514 (21000), 550 (4800), 591 (6700) and 650 (1500). HR ESI-TOF-MS (positive mode): *m*/*z* (% intensity): 807.0730 (100) $[M+H]^+$, calcd for $C_{40}H_{17}F_{10}N_4S_2$ = 807.0729.

P1Br: ^{1}H NMR (600 MHz, $CDCl_3$, 300 K): δ (ppm) 9.20 (d, 4H, J = 4.6 Hz; β-H), 8.82 (d, 4H, J = 4.6 Hz; β-H), 7.67 (dd, 2H, J_1 = 3.7 Hz, J_2 = 1.4 Hz; thienyl-H), 7.50 (dd, 2H, J_1 = 3.7 Hz, J_2 = 1.4 Hz; thienyl-H), and –2.80 (br s, 2H; inner NH); ^{19}F NMR (565 MHz, $CDCl_3$, 300 K): δ (ppm) –136.70 (dd, 4F, J_1 = 25.2 Hz, J_2 = 7.0 Hz; *o*-F), –152.76 (t, 2F, J = 22.0 Hz; *p*-F), and –161.60 (br t, 4H, J = 22.0 Hz; *m*-F). UV / vis (in CH_2Cl_2): λ_{max}[nm] (nomalized) = 421 (1.000), 515 (0.061), 551 (0.017), 591 (0.021) and 652 (0.004). HR ESI-TOF-MS (positive mode): *m*/*z* (% intensity): 964.8929 (100) $[M+H]^+$, calcd for $C_{40}H_{15}F_{10}N_4S_2Br_2$ = 964.8922.

General Procedure for the Synthesis of 5,15-bis(pentafluorophenyl)-10,20-bis(α-oligothienyl)porphyrins

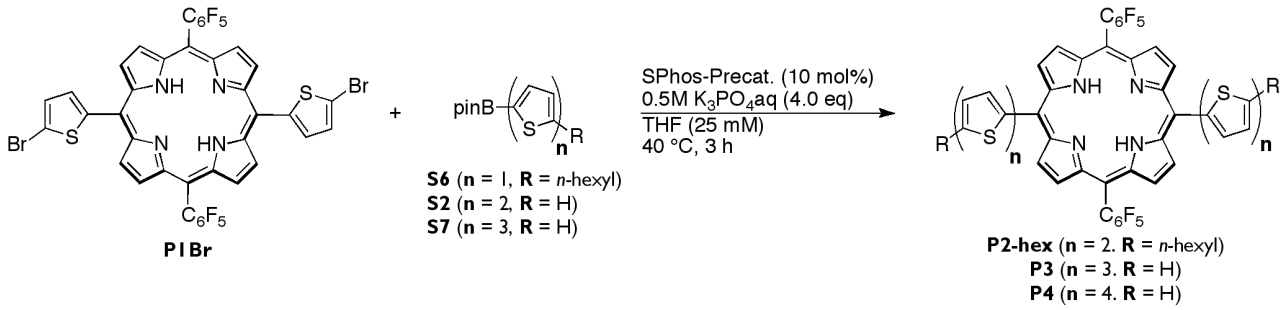

P1Br (48 mg, 50 μmol), the corresponding boronic acid pinacol ester (4.0 eq), **SPhos-Precat.** (3.6 mg, 10 mol%), and dry THF (2.0 mL; 25 mM) were added to a Schlenk tube. To the mixture, degassed 0.5 M K_3PO_4 aq. (0.40 mL; 4.0 eq) was added. The reaction mixture was stirred at 40 °C. After 3 h, the mixture was cooled to room temperature and CH_2Cl_2 was added to dissolve the solids. The organic phase was dried over Na_2SO_4. The solvent was removed under reduced pressure and the residue was purified by silica gel column chromatography (CH_2Cl_2 : *n*-hexane = 1:1) and recrystallization with CH_2Cl_2/MeOH to give **P2-hex** (52 mg, 91% yield) or **P3** (34 mg, 60% yield) or **P4** (20 mg, 31% yield) as brown or purple solids, respectively. (#**P2** (**n** = 2, R = H) was difficult to isolate because of its low solubility.)

P2-hex: ^{1}H NMR (600 MHz, $CDCl_3$, 300 K): δ (ppm) 9.28 (d, 4H, J = 4.6 Hz; β-H), 8.80 (d, 4H, J = 4.6 Hz; β-H), 7.80 (d, 2H, J = 3.7 Hz; thienyl-H), 7.53 (d, 2H, J = 3.7 Hz; thienyl-H), 7.25 (d, 2H, J = 3.7 Hz; thienyl-H), 7.68 (d, 2H, J = 3.7 Hz; thienyl-H), 2.90 (t, 4H, J = 7.7 Hz; hexyl-H), 1.77 (t, 4H, J = 7.7 Hz; hexyl-H), 1.53 (m, 4H; hexyl-H), 1.37 (m, 8H; hexyl-H), 0.93 (m, 6H; hexyl-H), and –2.70 (br s, 2H; inner NH); ^{19}F NMR (565 MHz, $CDCl_3$, 300 K): δ (ppm) –136.65 (dd, 4F, J_1 = 25.2 Hz, J_2 = 7.0 Hz; *o*-F), –152.02 (t, 2F, J = 22.0 Hz; *p*-F), and –160.73 (br t, 4H, J = 22.0 Hz; *m*-F). UV/vis (in CH_2Cl_2): λ_{max}[nm] (ε [$M^{-1}cm^{-1}$]) = 421 (150000), 519 (18000), 566 (10000), 591 (9800) and 659 (2500). HR ESI-TOF-MS (positive mode): *m*/*z* (% intensity): 1139.2363 (100) [*M*+H]$^+$, calcd for $C_{60}H_{45}F_{10}N_4S_4$ = 1139.2362.

P3: ^{1}H NMR (600 MHz, $CDCl_3$, 300 K): δ (ppm) 9.29 (d, 4H, J = 4.6 Hz; β-H), 8.82 (d, 4H, J = 4.6 Hz; β-H), 7.84 (d, 2H, J = 3.7 Hz; thienyl-H), 7.61 (d, 2H, J = 3.7 Hz; thienyl-H), 7.35 (d, 2H, J = 3.7 Hz; thienyl-H), 7.29 (m, 4H; thienyl-H), 7.22 (d, 2H, J = 3.7 Hz; thienyl-H), 7.09 (m, 2H; thienyl-H), and –2.67 (br s, 2H; inner NH); ^{19}F NMR (565 MHz, $CDCl_3$, 300 K): δ (ppm) –136.68 (dd, 4F, J_1 = 25.2 Hz, J_2 = 7.0 Hz; *o*-F), –151.95 (t, 2F, J = 22.0 Hz; *p*-F), and –160.70 (br t, 4H, J = 22.0 Hz; *m*-F). UV/vis (in CH_2Cl_2): λ_{max}[nm] (ε [$M^{-1}cm^{-1}$]) = 418 (180000), 517 (21000), 567 (13000), 591 (12000) and 657 (2200). HR ESI-TOF-MS (positive mode): *m*/*z* (% intensity): 1135.0219 (100) [*M*+H]$^+$, calcd for $C_{56}H_{25}F_{10}N_4S_6$ = 1135.0238.

P4: ^{1}H NMR (600 MHz, $CDCl_3$, 300 K): δ (ppm) 9.30 (d, 4H, J = 4.6 Hz; β-H), 8.82 (d, 4H, J = 4.6 Hz; β-H), 7.84 (d, 2H, J = 3.7 Hz; thienyl-H), 7.62 (d, 2H, J = 3.7 Hz; thienyl-H), 7.36 (d, 2H, J = 3.7 Hz; thienyl-H), 7.23 (m, 6H; thienyl-H), 7.19 (d, 2H, J = 3.7 Hz; thienyl-H), 7.15 (d, 2H, J = 3.7 Hz; thienyl-H), 7.05 (dd, 2H, J_1 = 5.0 Hz,

J_2 = 3.7 Hz; thienyl-H), and –2.67 (br s, 2H; inner NH); ^{19}F NMR (565 MHz, $CDCl_3$, 300 K): δ (ppm) –136.66 (dd, 4F, J_1 = 25.2 Hz, J_2 = 7.0 Hz; *o*-F), –151.93 (t, 2F, J = 22.0 Hz; *p*-F), and –160.69 (br t, 4H, J = 22.0 Hz; *m*-F). UV/vis (in CH_2Cl_2): λ_{max}[nm] (ε [$M^{-1}cm^{-1}$]) = 419 (160000), 515 (22000; shoulder), 571 (13000), 584 (13000) and 659 (2200). HR ESI-TOF-MS (negative mode): *m*/*z* (% intensity): 1297.9887 (100) $[M]^-$, calcd for $C_{64}H_{28}F_{10}N_4S_8$ = 1297.9914.

II. *Supporting Figures and Tables*

1. Absorption Spectra

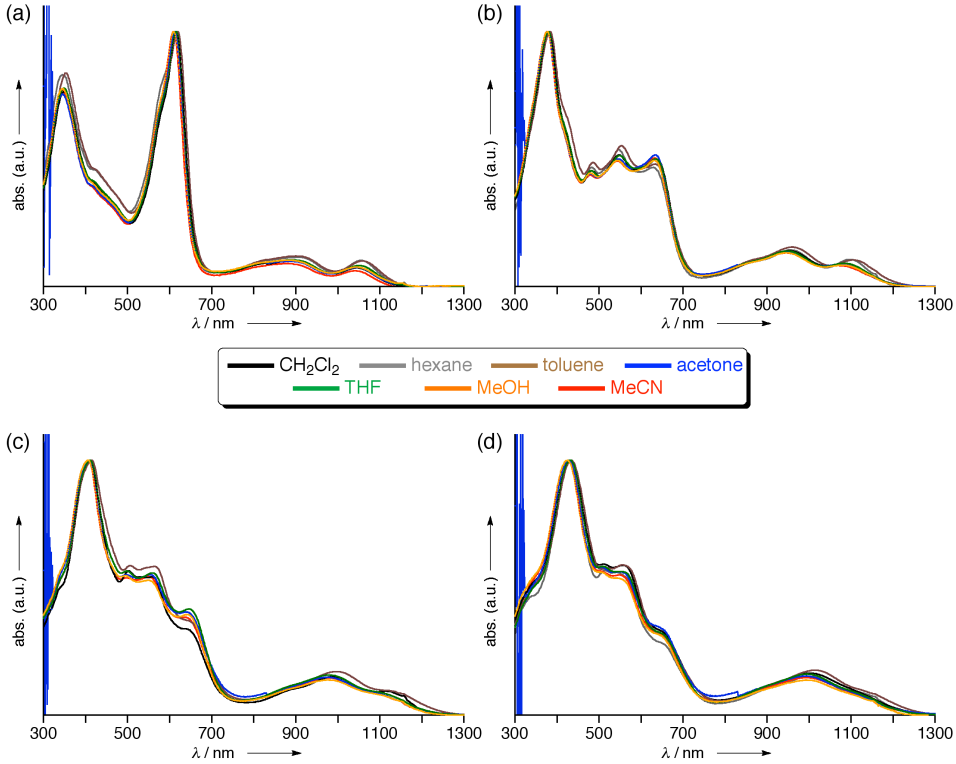

Figure S1. UV/Vis/NIR absorption spectra of **T1–T4** in various solvents.

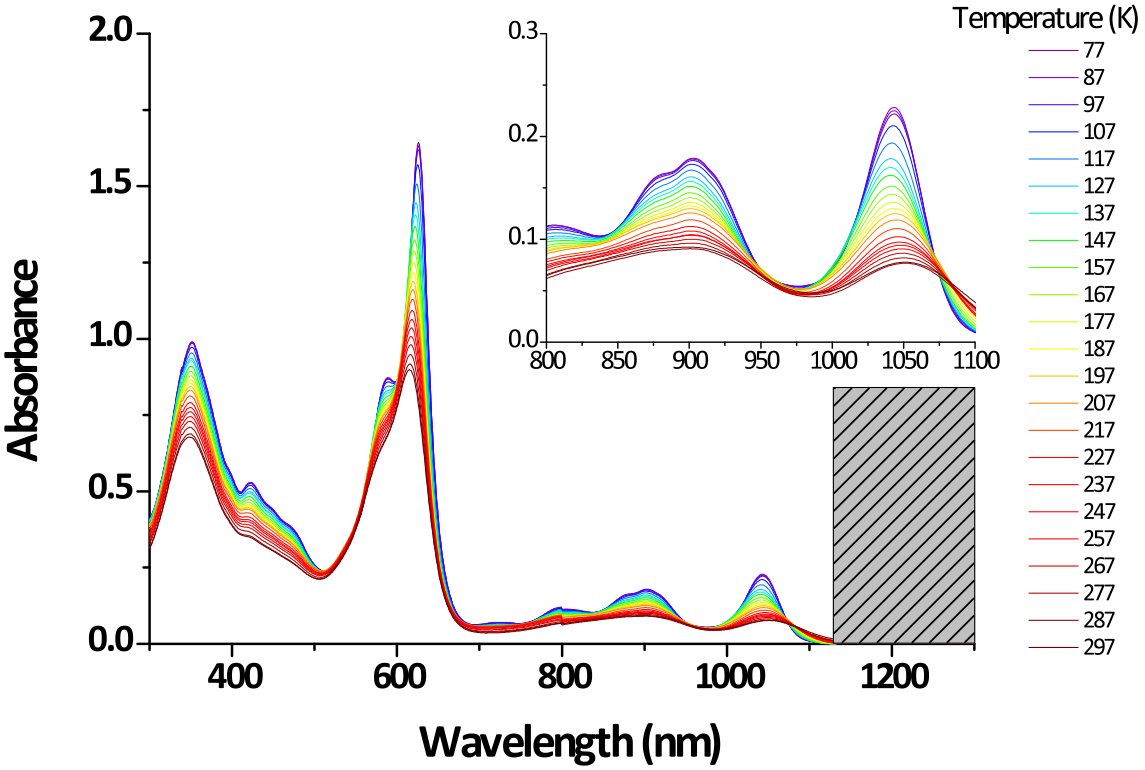

Figure S2. Temperature dependent UV/Vis/NIR absorption spectra of **T1** in 2-methyl THF (T = 77–297 K).

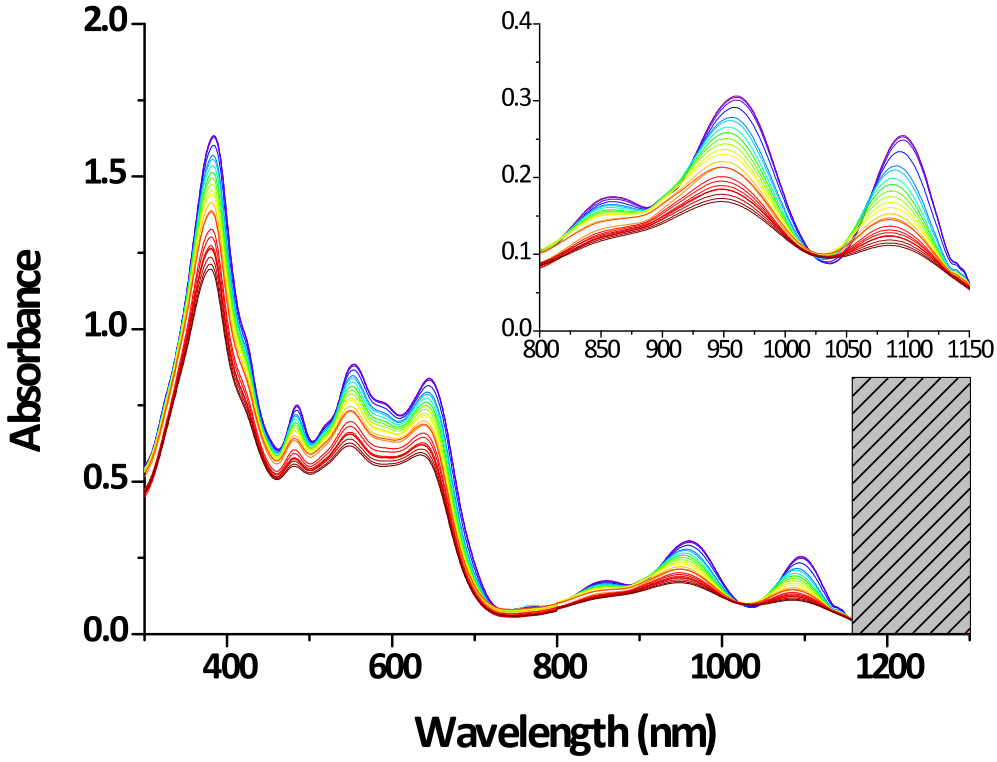

Figure S3. Temperature dependent UV/Vis/NIR absorption spectra of **T2** in 2-methyl THF (T = 77–297 K).

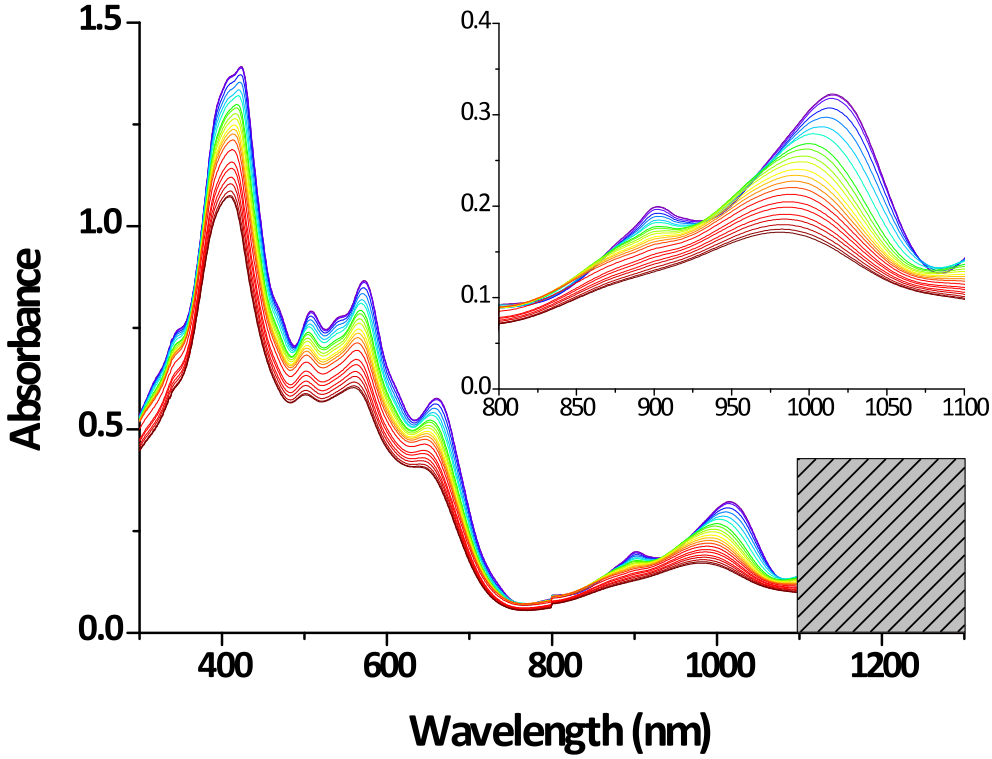

Figure S4. Temperature dependent UV/Vis/NIR absorption spectra of **T3** in 2-methyl THF (T = 77–297 K).

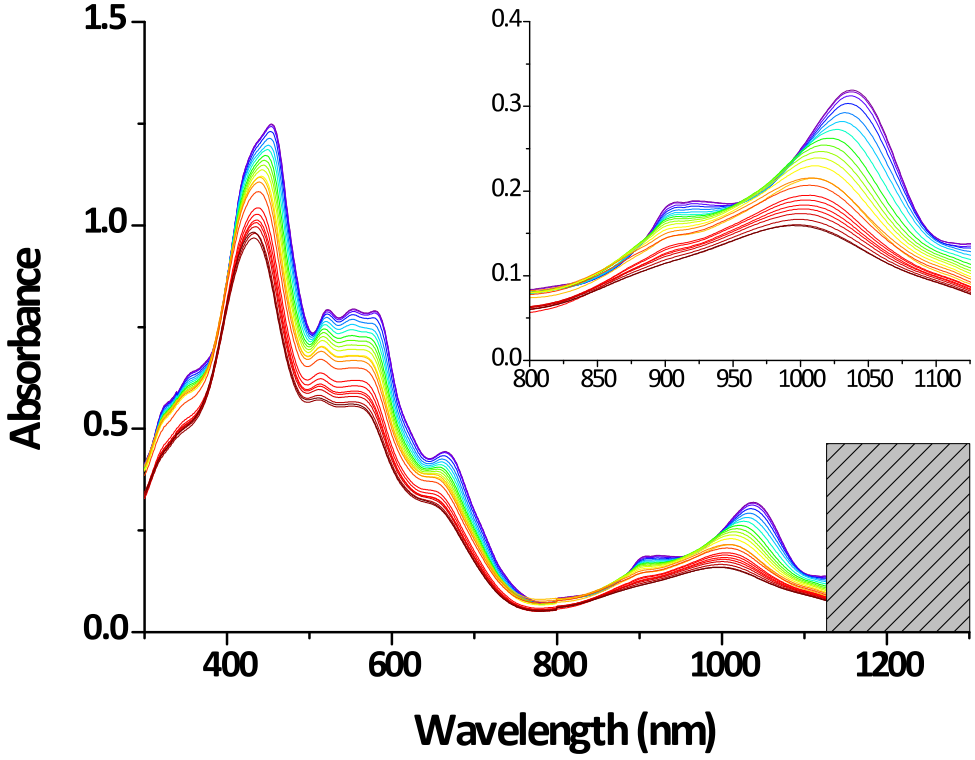

Figure S5. Temperature dependent UV/Vis/NIR absorption spectra of **T4** in 2-methyl THF (T = 77–297 K).

2. ^{1}H and ^{19}F NMR Spectra

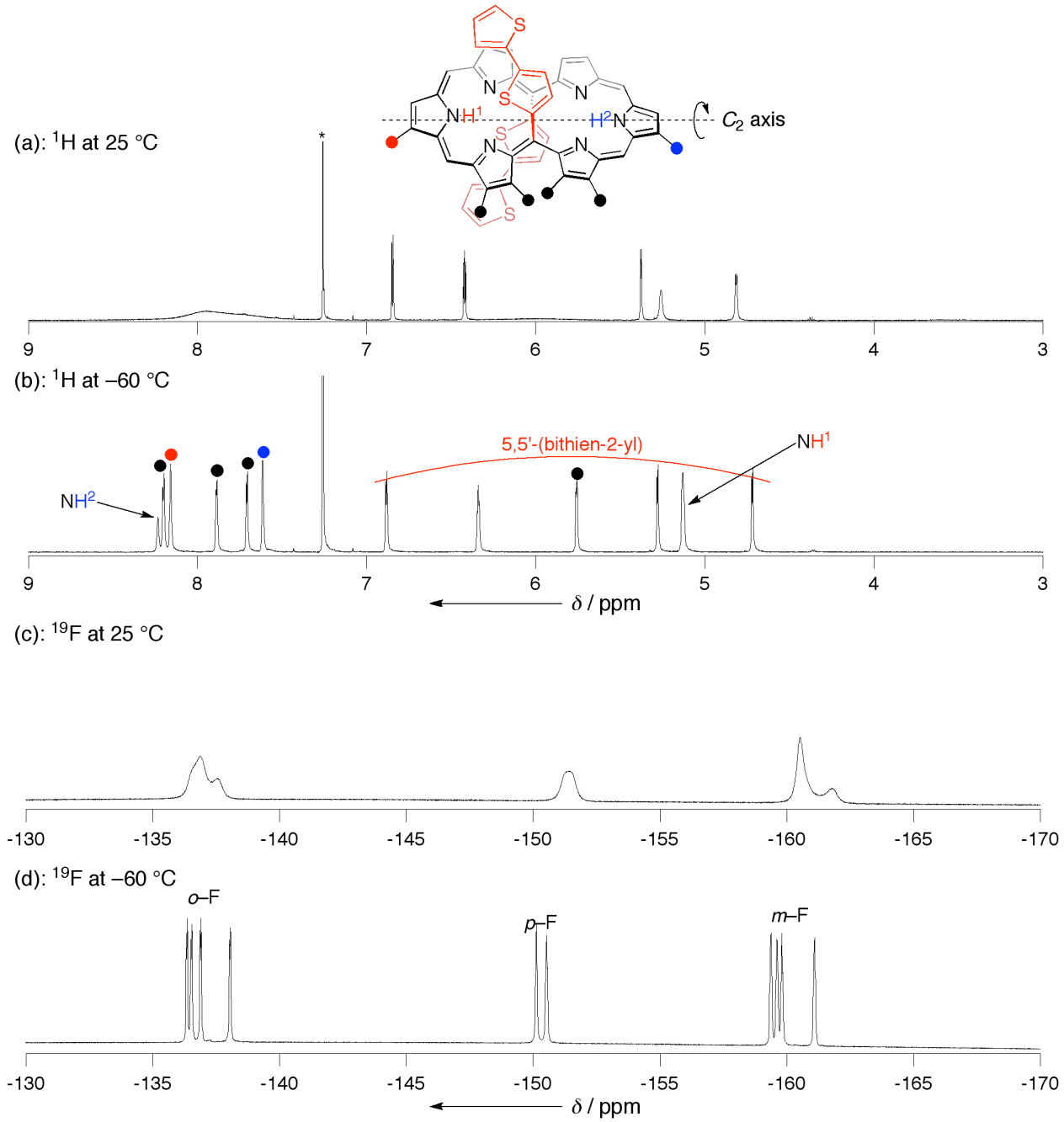

Figure S6. Variable temperature ^{1}H and ^{19}F NMR spectra of **T2** in $CDCl_3$. *: Residual solvent peaks.

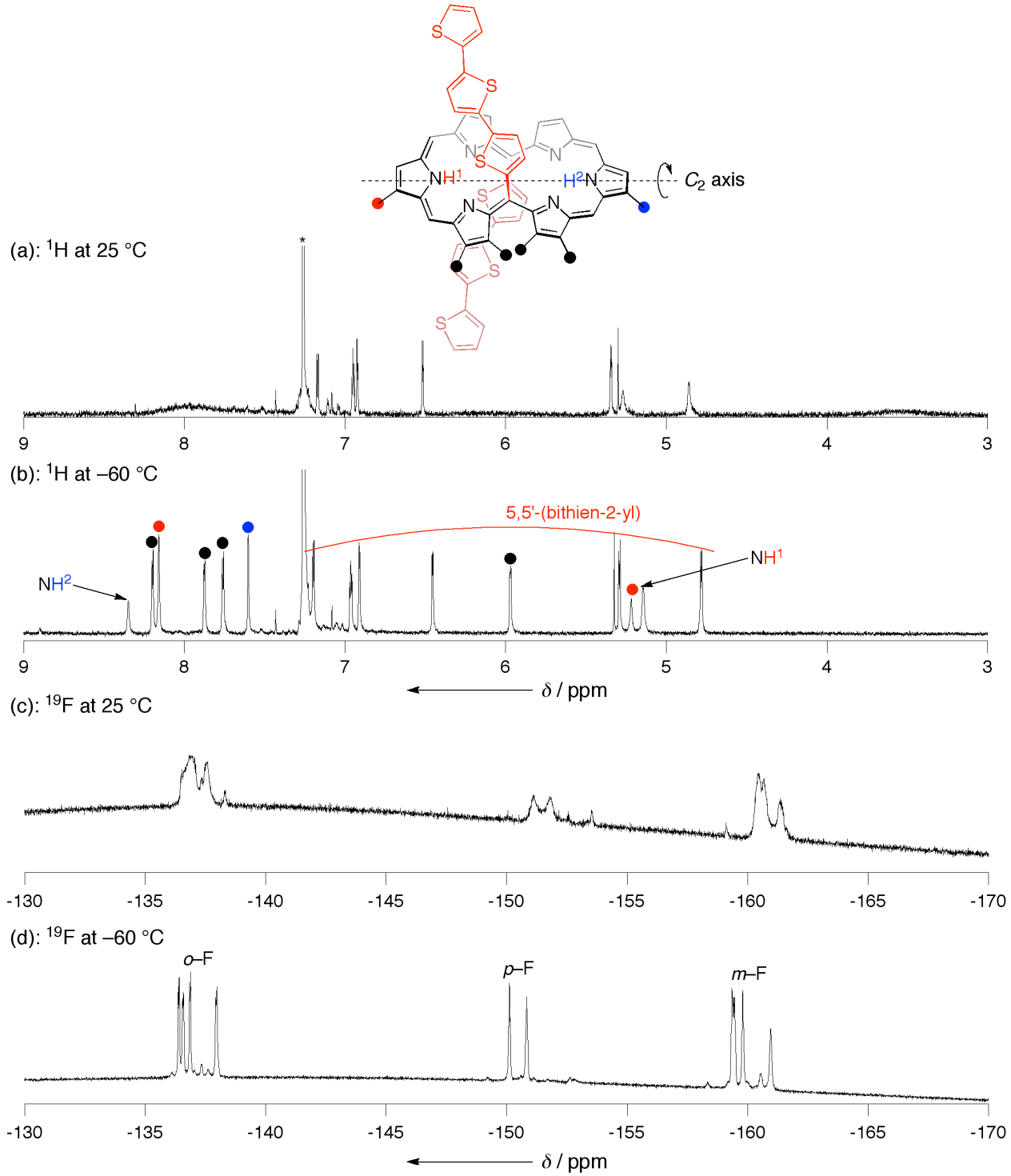

Figure S7. Variable temperature ^{1}H and ^{19}F NMR spectra of **T3** in $CDCl_3$. *: Residual solvent peaks.

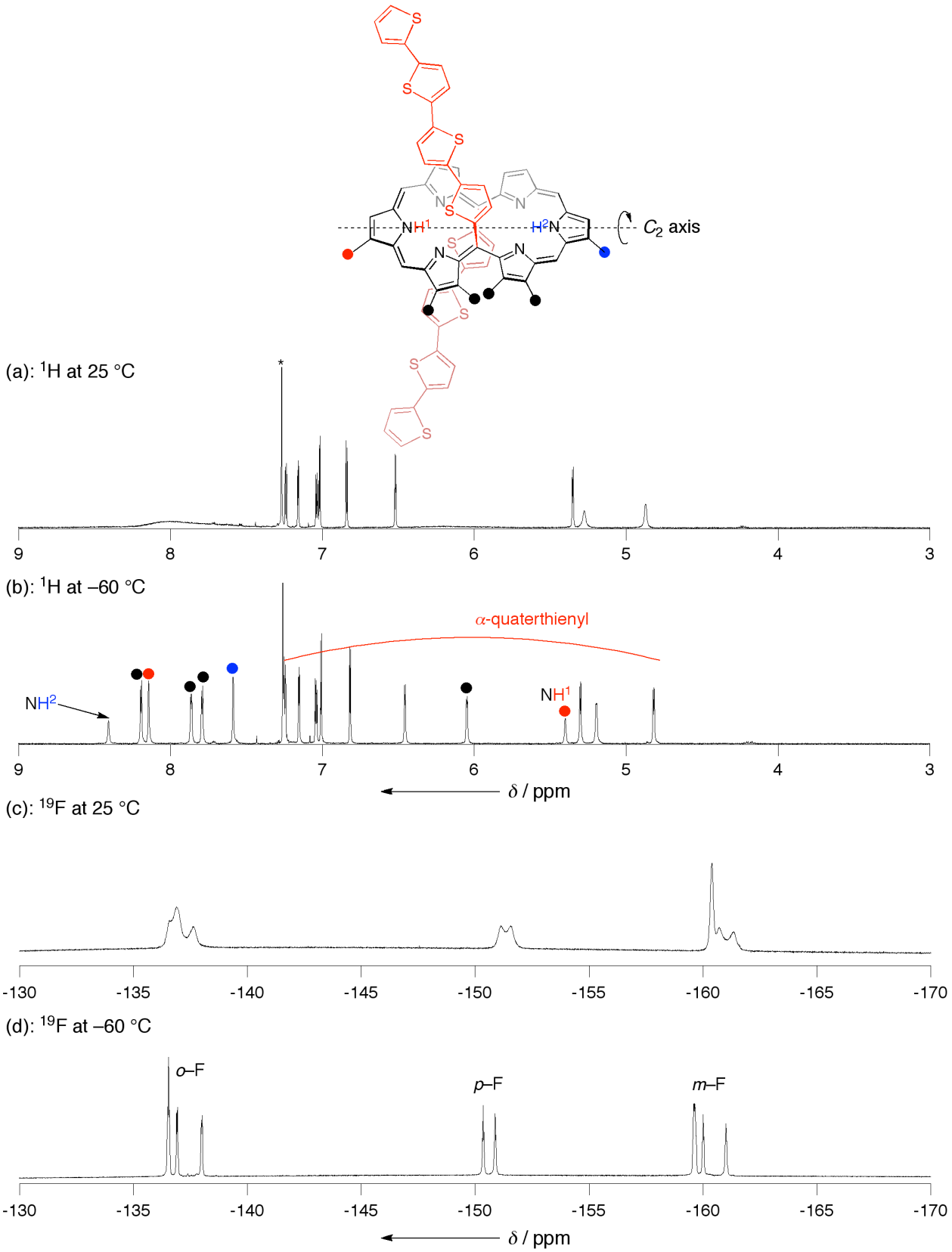

Figure S8. Variable temperature ^{1}H and ^{19}F NMR spectra of **T4** in $CDCl_3$. *: Residual solvent peaks.

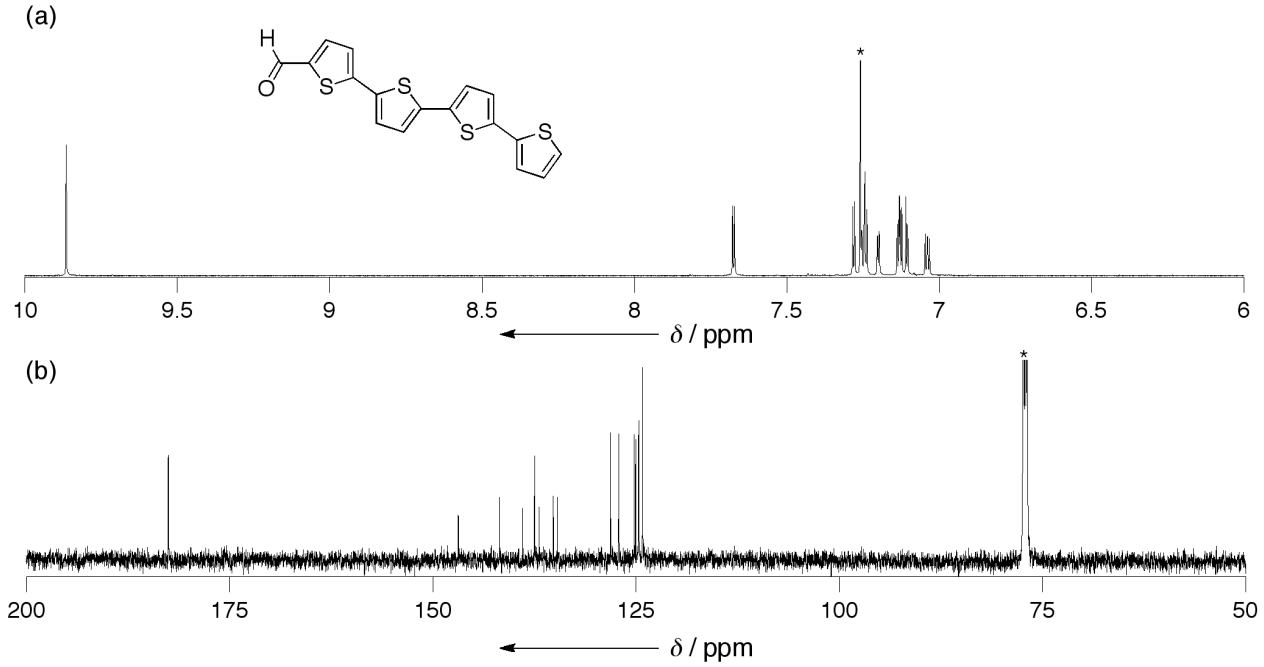

Figure S9. (a) ^{1}H and (b) ^{13}C NMR spectra of **s3** in $CDCl_3$ at 25 °C. *: Residual solvent peaks.

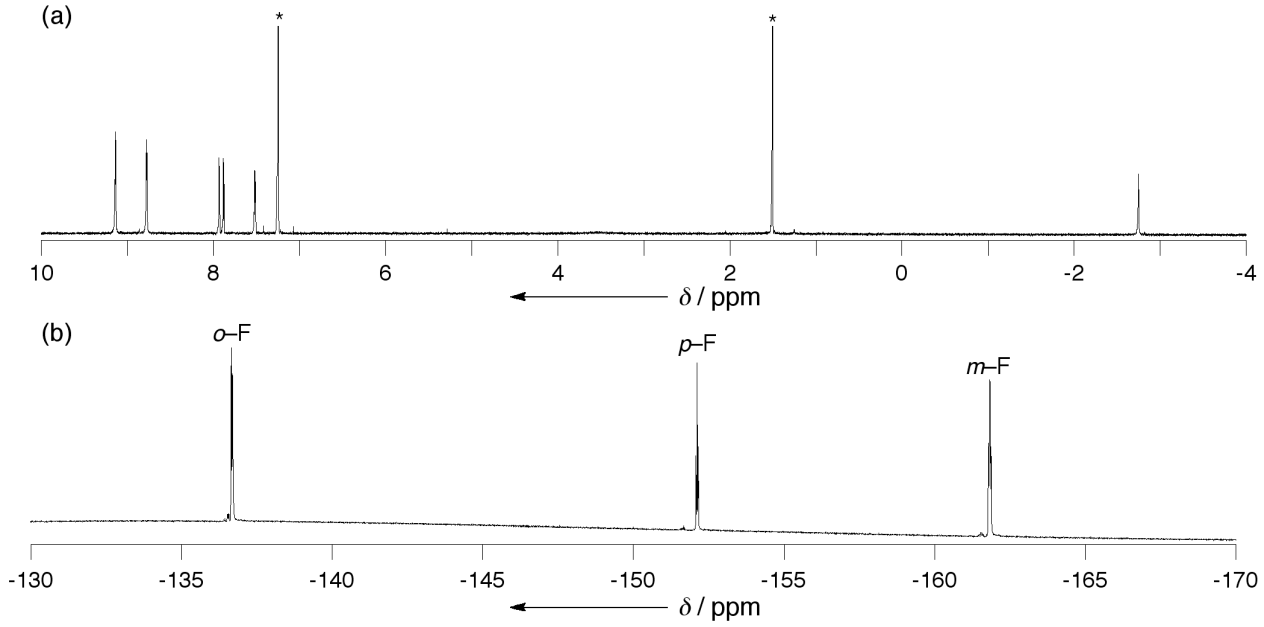

Figure S10. (a) ^{1}H and (b) ^{19}F NMR spectra of **P1** in $CDCl_3$ at 25 °C. *: Residual solvent peaks.

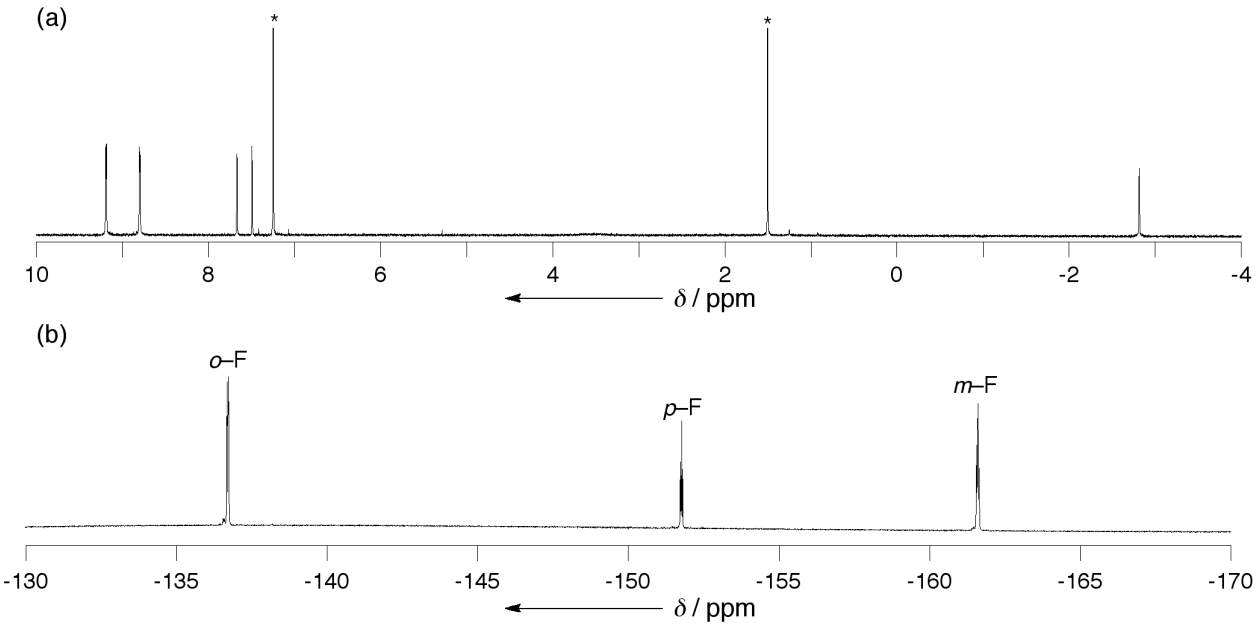

Figure S11. (a) ^{1}H and (b) ^{19}F NMR spectra of **P1Br** in $CDCl_3$ at 25 °C. *: Residual solvent peaks.

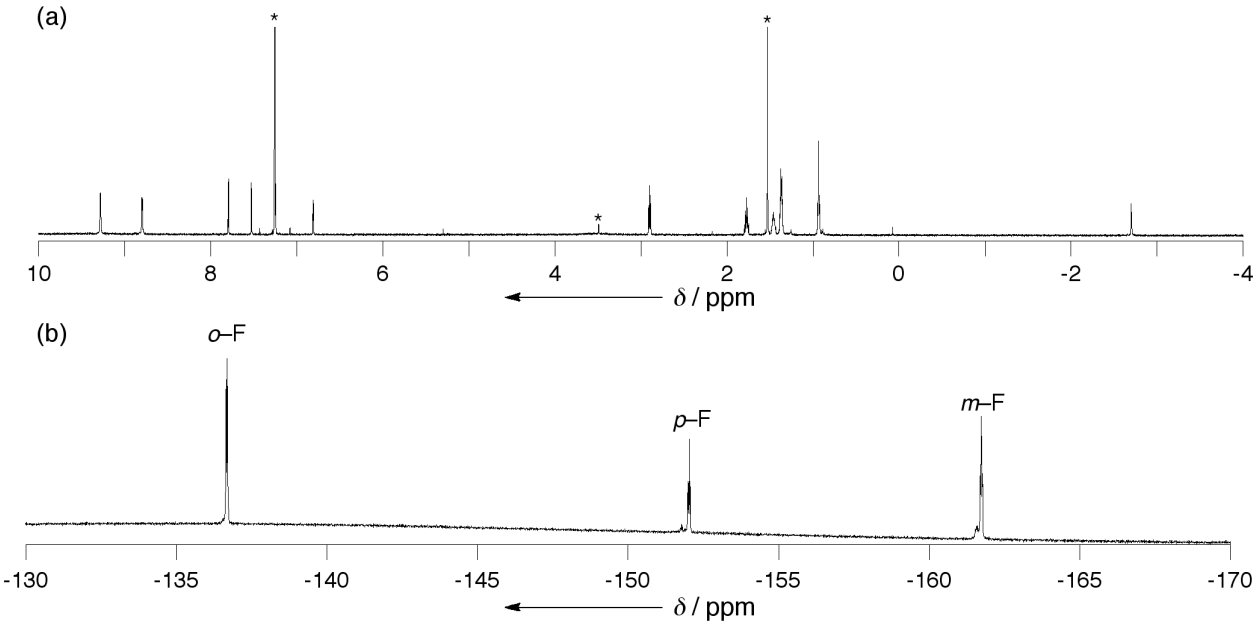

Figure S12. (a) ^{1}H and (b) ^{19}F NMR spectra of **P2** in $CDCl_3$ at 25 °C. *: Residual solvent peaks.

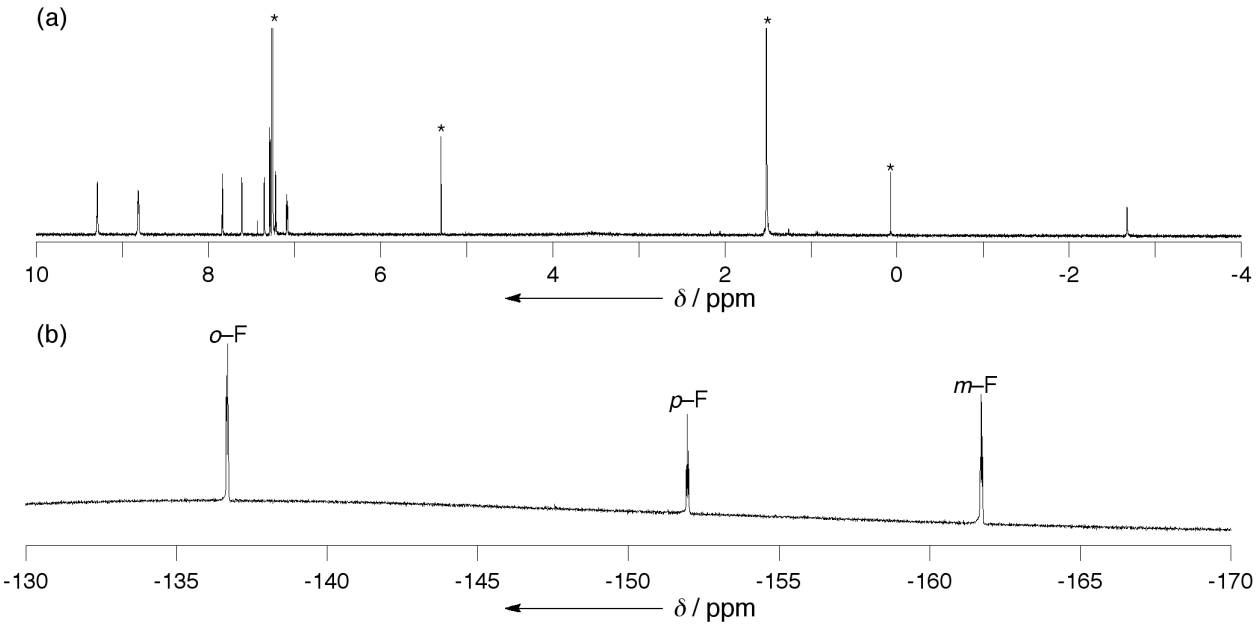

Figure S13. (a) ^{1}H and (b) ^{19}F NMR spectra of **P3** in $CDCl_3$ at 25 °C. *: Residual solvent peaks.

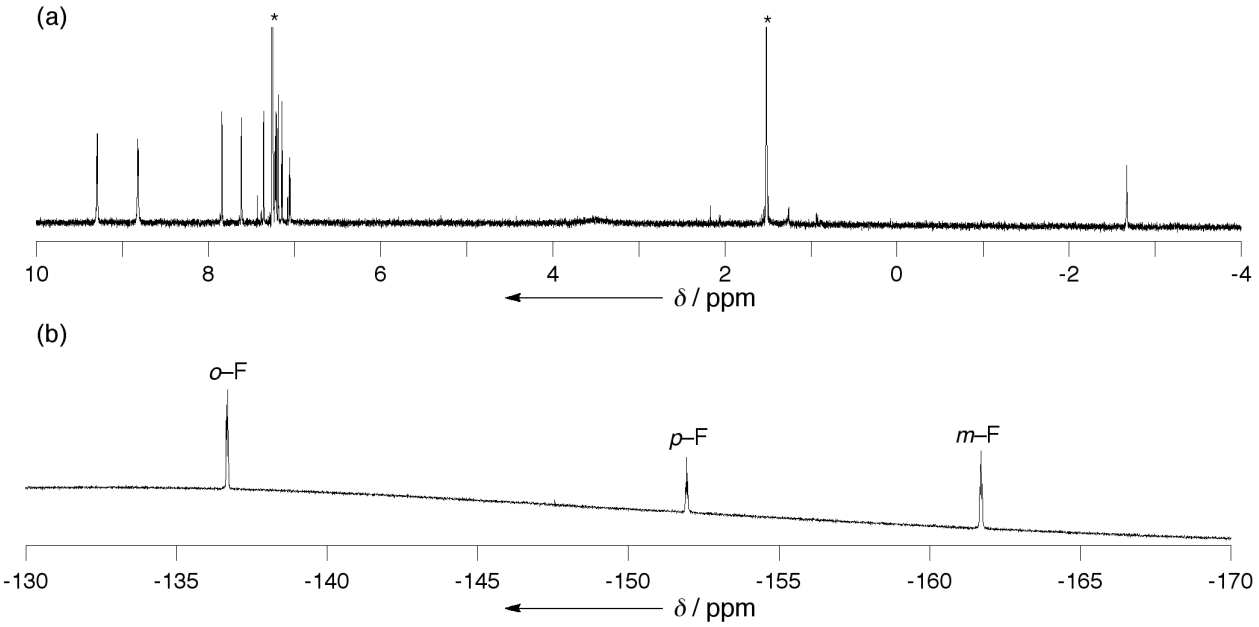

Figure S14. (a) ^{1}H and (b) ^{19}F NMR spectra of **P4** in $CDCl_3$ at 25 °C. *: Residual solvent peaks.

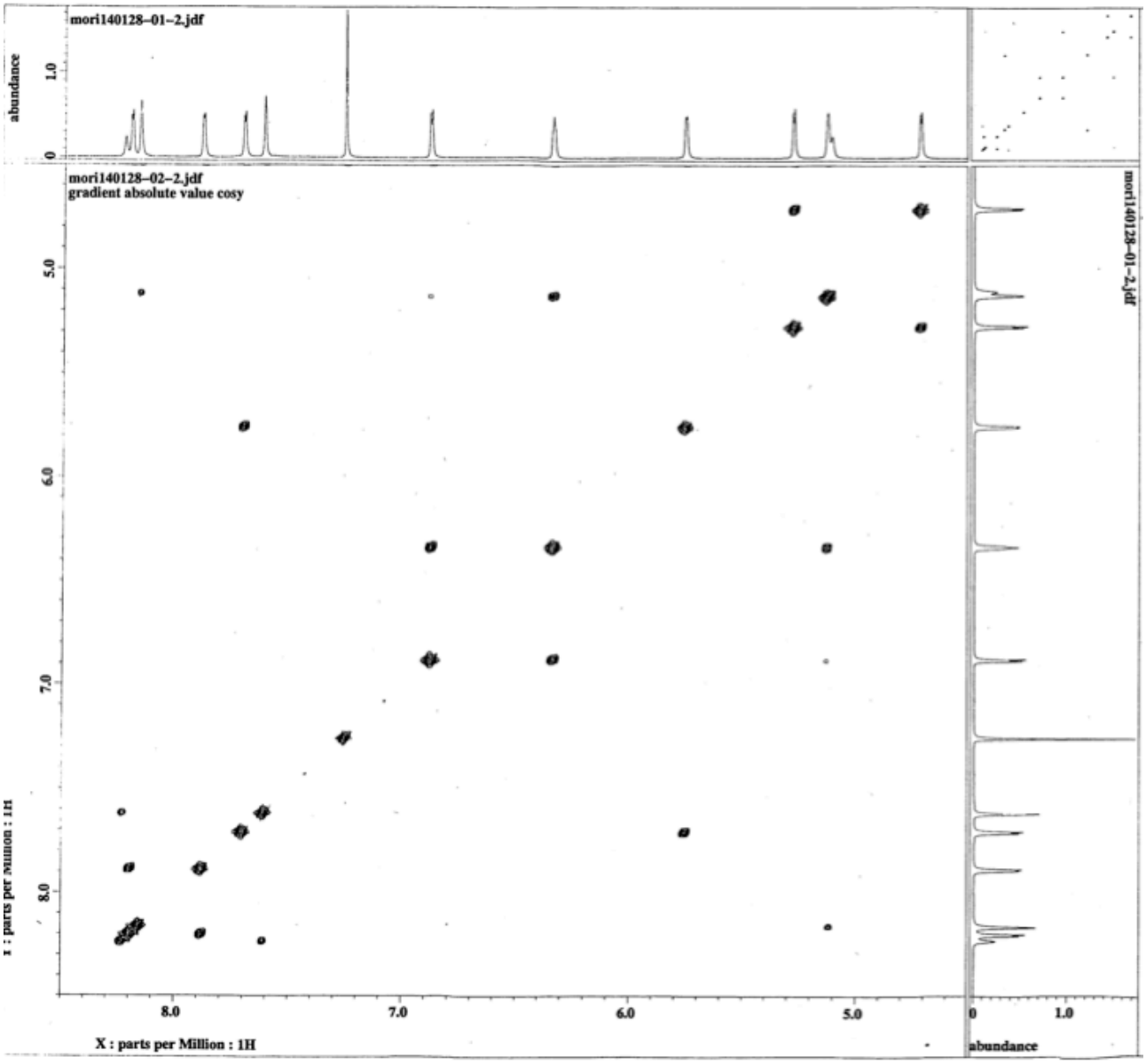

Figure S15. ^{1}H–^{1}H COSY spectrum of **T2** in $CDCl_3$ at –60 °C.

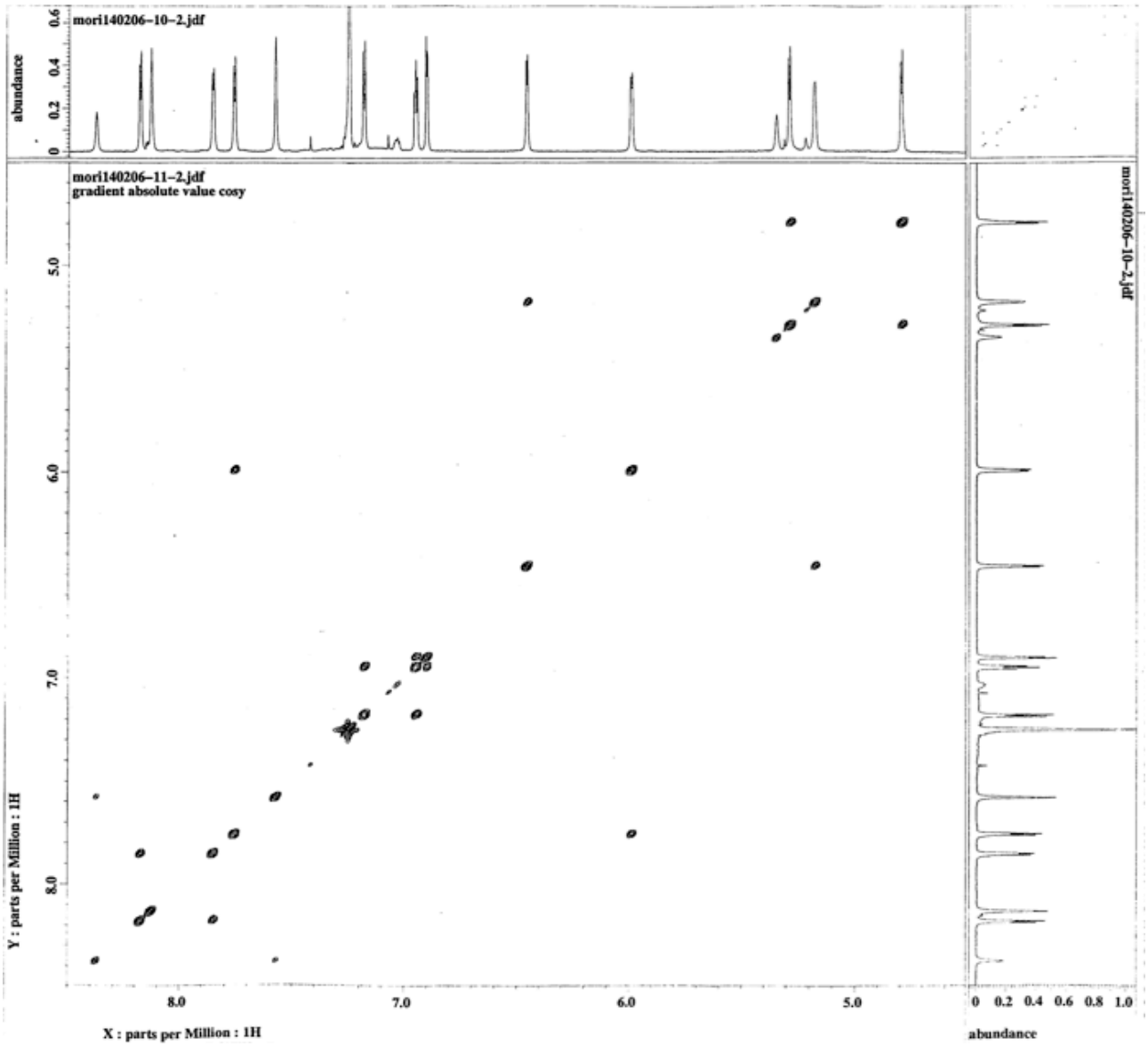

Figure S16. ^{1}H–^{1}H COSY spectrrum of **T3** in $CDCl_3$ at –40 °C.

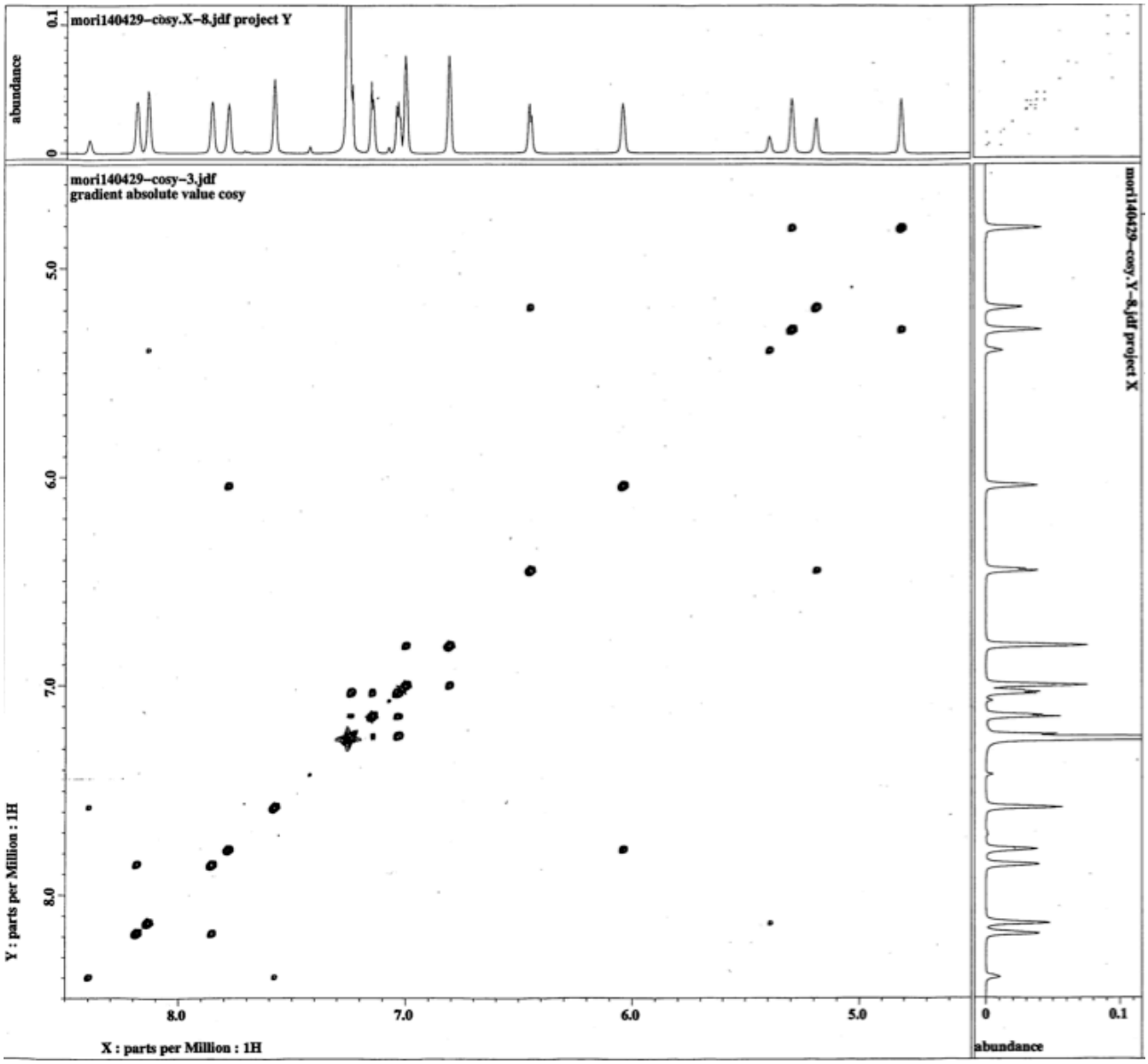

Figure S17. ^{1}H–^{1}H COSY spectrrum of **T4** in $CDCl_3$ at –40 °C.

3. ESI-TOF-MS Data

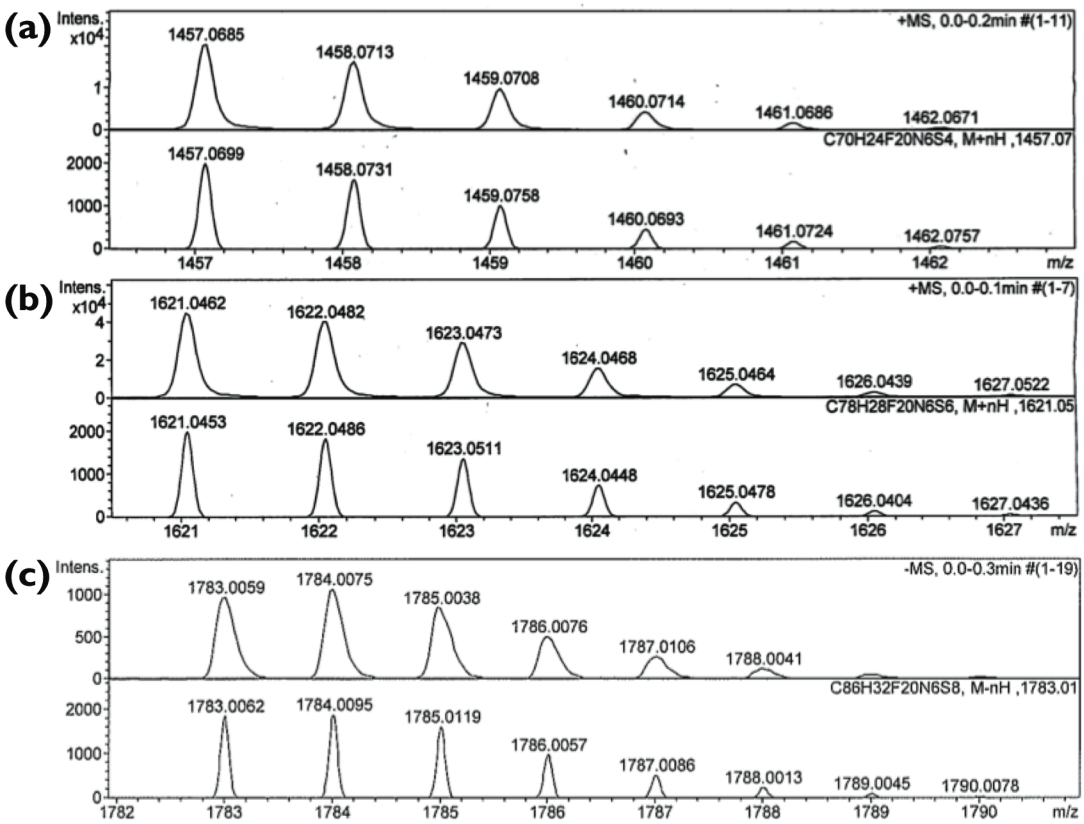

Figure S18. Observed (top) and simulated (bottom) high-resolution ESI-TOF-MS of (a): **T2**, (b): **T3**, and (c): **T4** in MeCN.

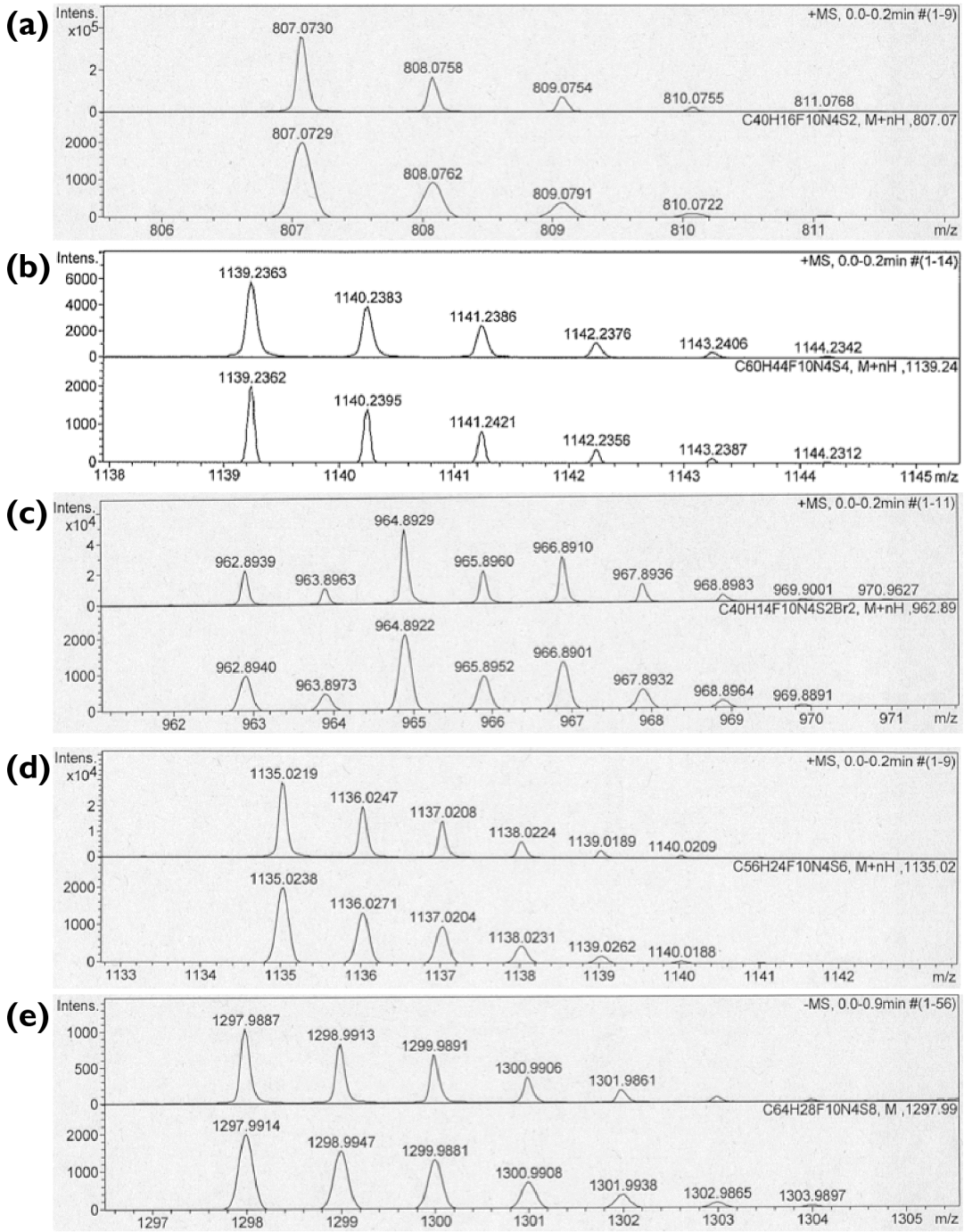

Figure S19. Observed (top) and simulated (bottom) high-resolution ESI-TOF-MS of (a): **P1**, (b): **P2**, (c): **P1Br**, (d): **P3**, and (e): **P4** in MeCN.

4. Cyclic Voltammograms

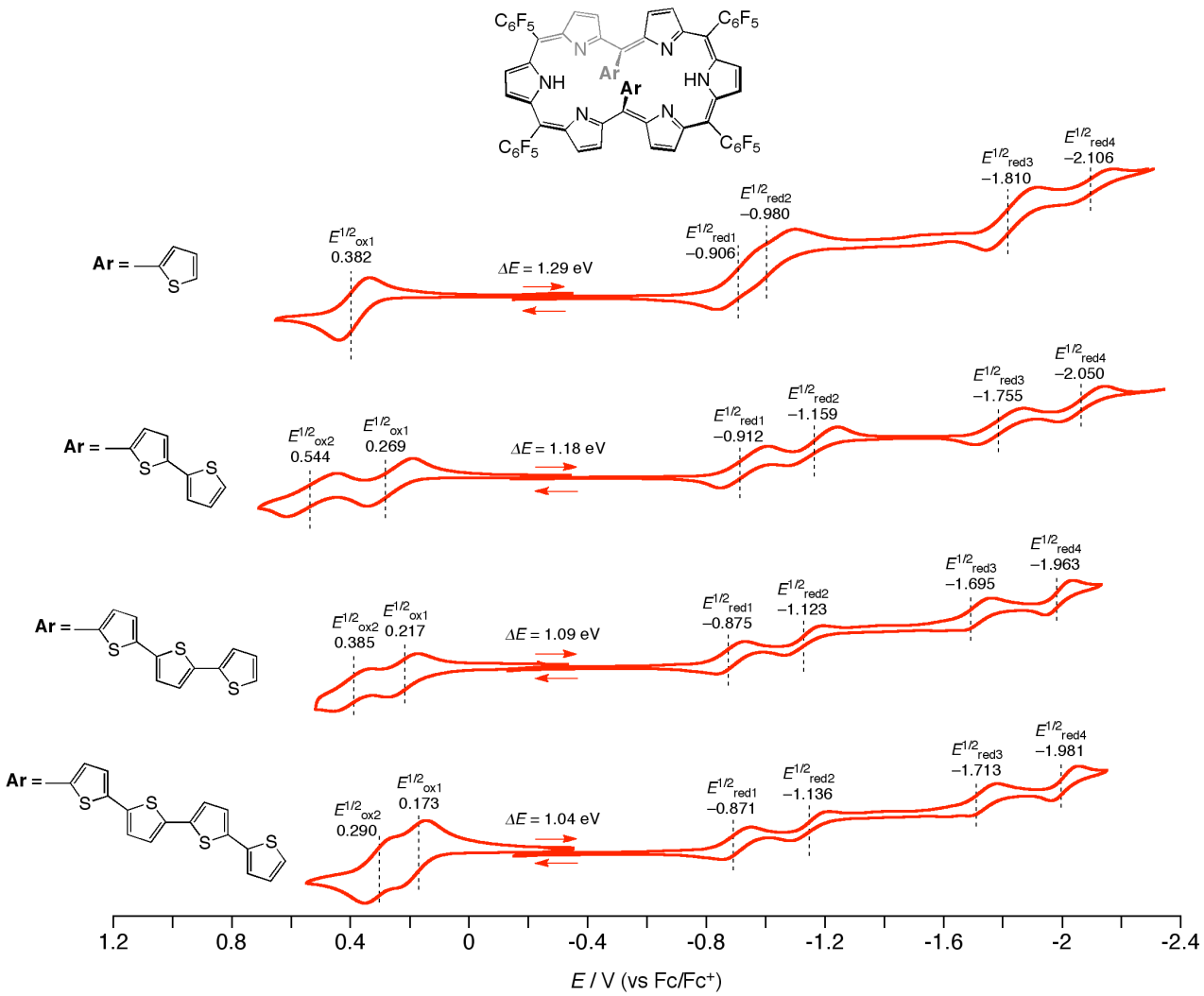

Figure S20. Cyclic voltammogram (CV; red line) of **T1–T4**.

Table S1. Electrochemical potentials[a] and estimated HOMO–LIMO gaps (ΔE) of **T1–T4**.

	$E^{1/2}_{ox2}$	$E^{1/2}_{ox1}$	$E^{1/2}_{red1}$	$E^{1/2}_{red2}$	$E^{1/2}_{red3}$	$E^{1/2}_{red4}$	ΔE [eV]
T1	–	0.38	–0.91	–0.98	–1.81	–2.11	1.29
T2	0.54	0.27	–0.91	–1.16	–1.76	–2.05	1.18
T3	0.39	0.22	–0.88	–1.12	–1.70	–1.96	1.09
T4	0.29	0.17	–0.87	–1.14	–1.71	–1.98	0.98

[a] Measured in CH_2Cl_2, potentials [V] vs ferrocene/ferrocenium ion. Scan rate, 0.05 Vs^{-1}; working electrode, Pt; counter electrode, Pt wire; supporting electrolyte, 0.1 $_M$ Bu_4NPF_6.

5. Crystal Data

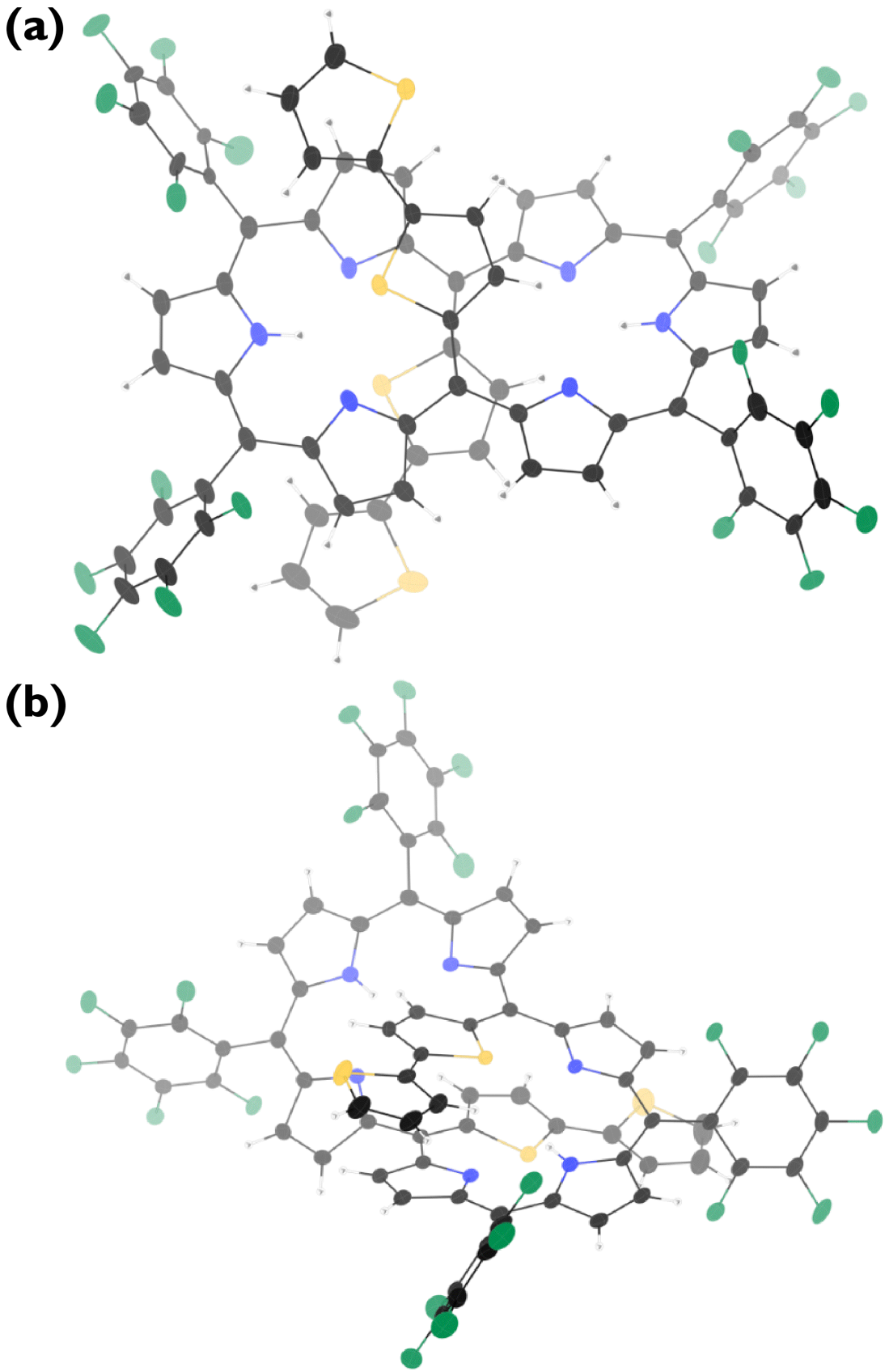

Figure S21. X-Ray crystal structure of **T2**. Solvent molecules are omitted for clarity. The thermal ellipsoids represent 30% probability level.

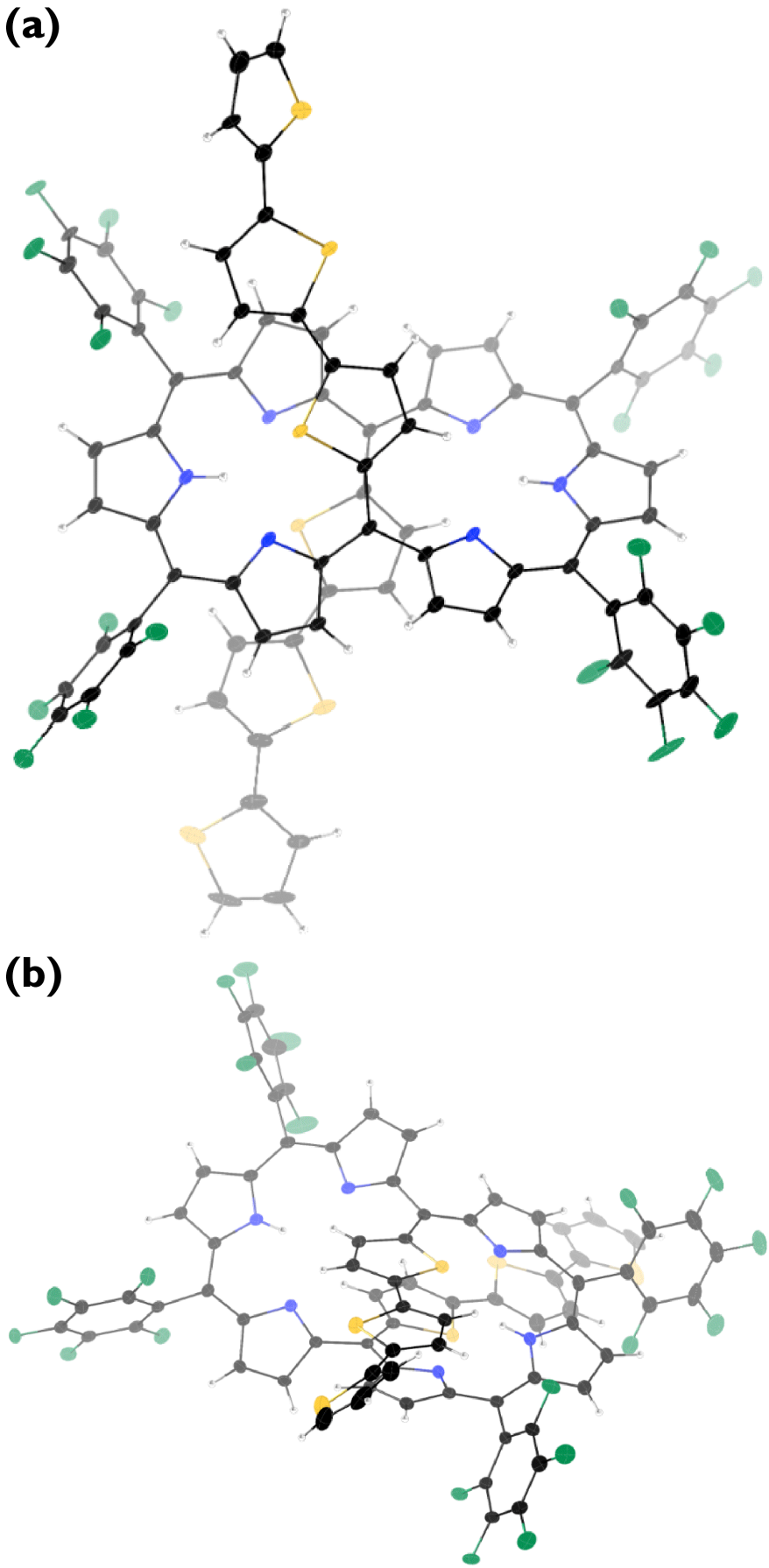

Figure S22. X-Ray crystal structure of **T3**. Solvent molecules are omitted for clarity. The thermal ellipsoids represent 30% probability level.

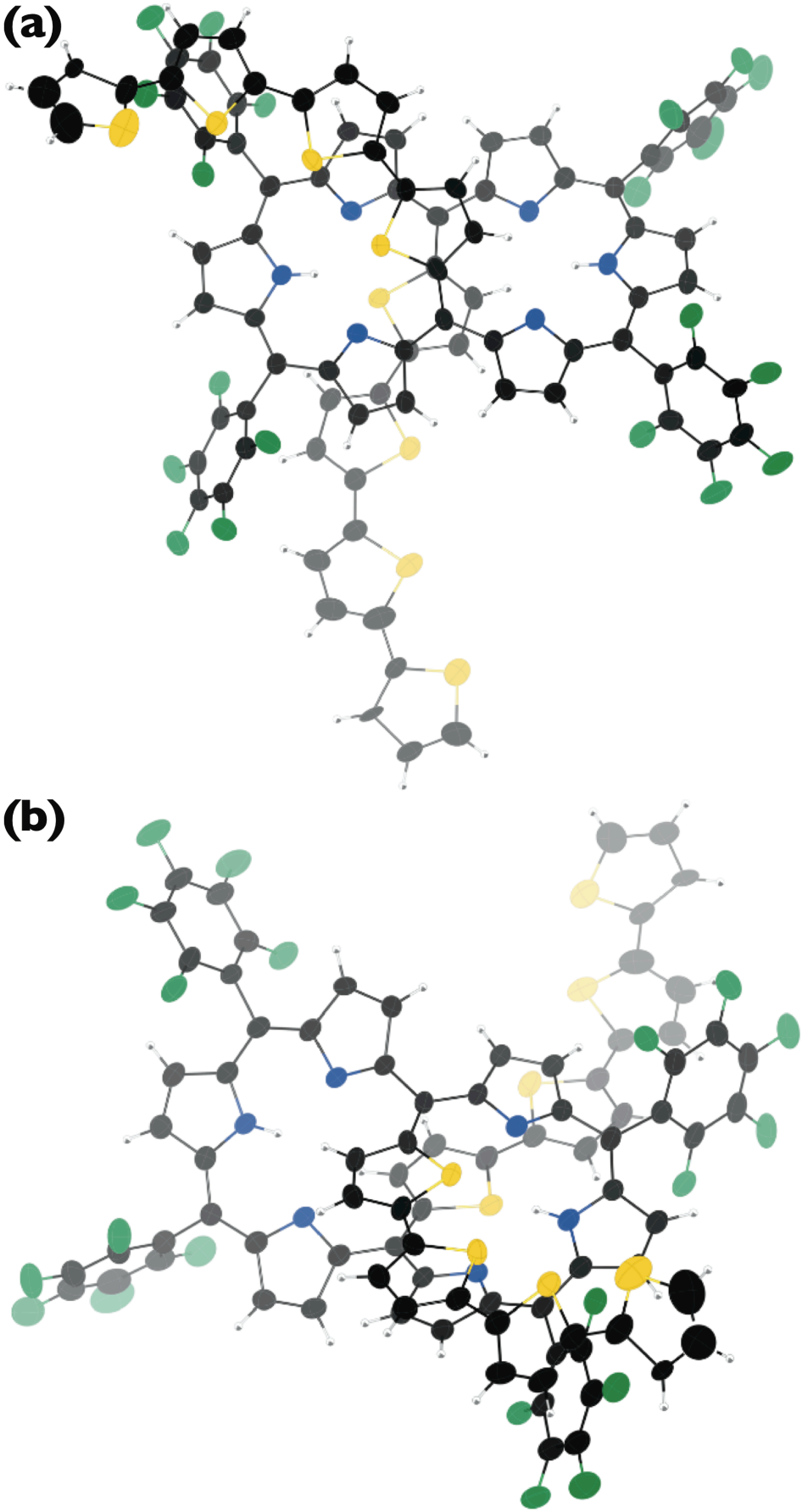

Figure S23. X-Ray crystal structure of **T4**. Solvent molecules are omitted for clarity. The thermal ellipsoids represent 30% probability level.

Table S2. Crystal data for **T2**, **T3**, and **T4**.

	T2	**T3**	**T4**
formula	$2(C_{70}H_{24}F_{20}N_6S_4)$	$C_{78}H_{28}F_{20}N_6S_6$	$2(C_{86}H_{32}F_{20}N_6S_8)$,
	$1.84(C_6H_{14})$	$0.51(C_7H_{16})$, C_7,	$2(C_7H_{16})$, $0.44C_7$,
	$1.10(CH_2Cl_2)$	$1.89(CH_2Cl_2)$	$1.53(CCl_3)$, O
Solvent	CH_2Cl_2	CH_2Cl_2	$CHCl_3$
	n-hexane	*n*-heptane	*n*-heptane
M_r	3165.36	1882.68	4006.31
T [K]	93	93	93
crystal system	triclinic	monoclinic	triclinic
space group	P-1	$C2/c$	P-1
	(No. 2)	(No. 15)	(No. 2)
a [Å]	18.9073(16)	49.998(16)	17.2734(8)
b [Å]	20.7452(6)	12.402(3)	18.9028(5)
c [Å]	21.091(2)	35.242(11)	30.1289(17)
α [°]	67.38(2)	–	105.000(14)
β [°]	77.21(2)	131.613(5)	92.92(2)
γ [°]	65.257(13)	–	107.23(3)
V [Å^3]	6917.2(9)	16338(8)	8988.7(7)
Z	2	8	2
ρ_{calcd} [gcm^{-3}]	1.520	1.531	1.481
R_1 [$I > 2\sigma(I)$]	0.0639	0.0850	0.1104
wR_2 [all data]	0.1805	0.2299	0.3750
GOF	1.042	1.034	1.073
CCDC Number	1025770	1025771	1025772

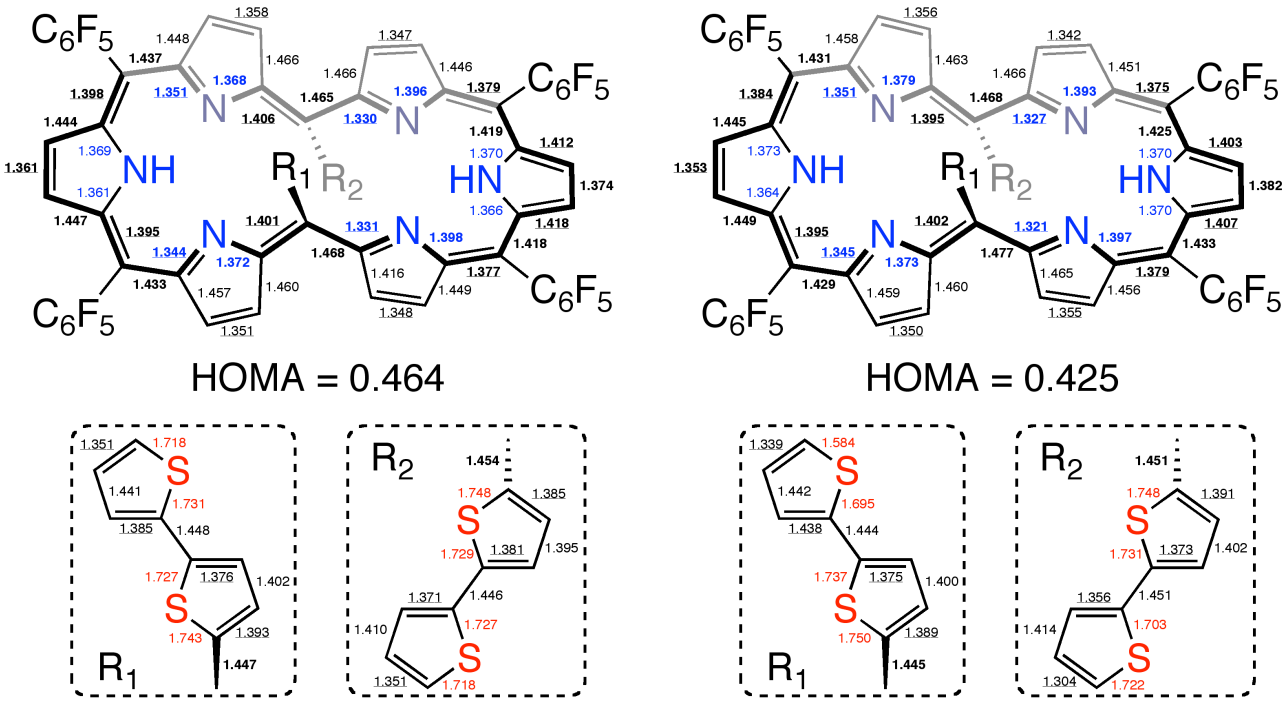

Figure S24. Selected bond length and HOMA value of **T2** in the packing structure. #The unit cell contains two different hexaphyrins. The tripyrrodimethene units on the left half are included in the helical structure.

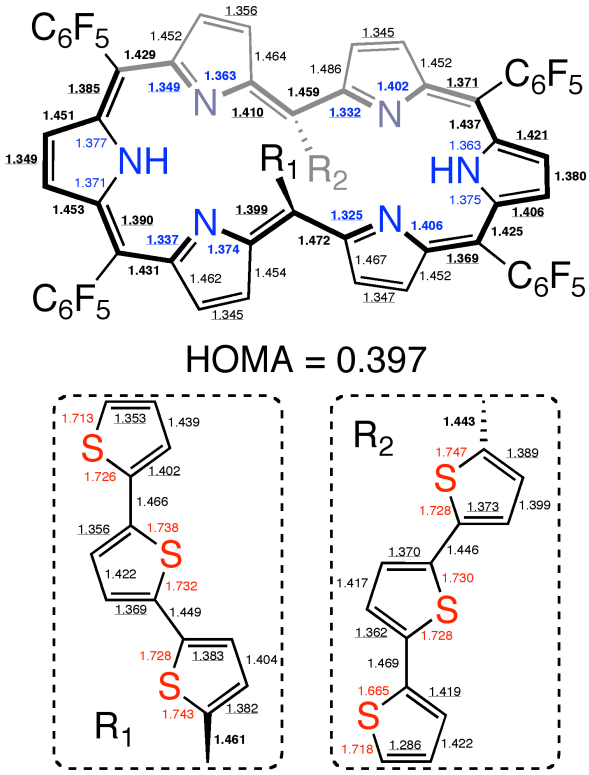

Figure S25. Selected bond length and HOMA value of **T3** in the packing structure. The tripyrrodimethene unit on the left half is included in the helical structure.

6. DFT Calculations

All calculations were carried out using the Gaussian *09* program.[S1] Initial geometries were obtained from X-ray structures. All structures were fully optimized without any symmetry restriction. The calculations were performed by the density functional theory (DFT) method with restricted B3LYP (Becke's three-parameter hybrid exchange functionals and the Lee-Yang-Parr correlation functional),[S2,S3] employing a basis set 6-31G(d) for C, H, N, and F. The NICS values and absolute ^{1}H shielding values were obtained with the GIAO method at the B3LYP/6-31G(d) level. The ^{1}H chemical shift values were calculated relative to $CHCl_3$ (δ = 7.26 ppm, absolute shielding: 24.94 ppm). The global ring centers for the NICS values were designated at the nonweighted means of the carbon and nitrogen coordinates on the peripheral positions of macrocycles. In addition, NICS values were also calculated on centers of other local cyclic structures as depicted in the following figures.

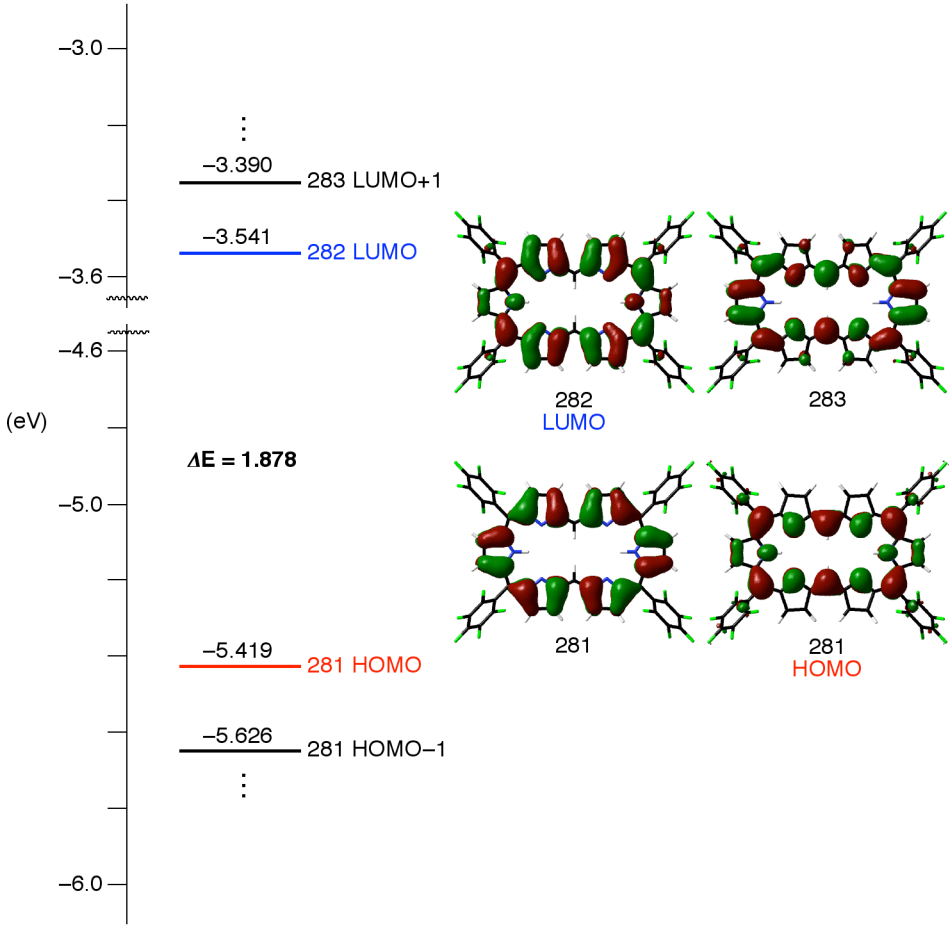

Figure S26. Frontier orbital diagrams of **T0**.

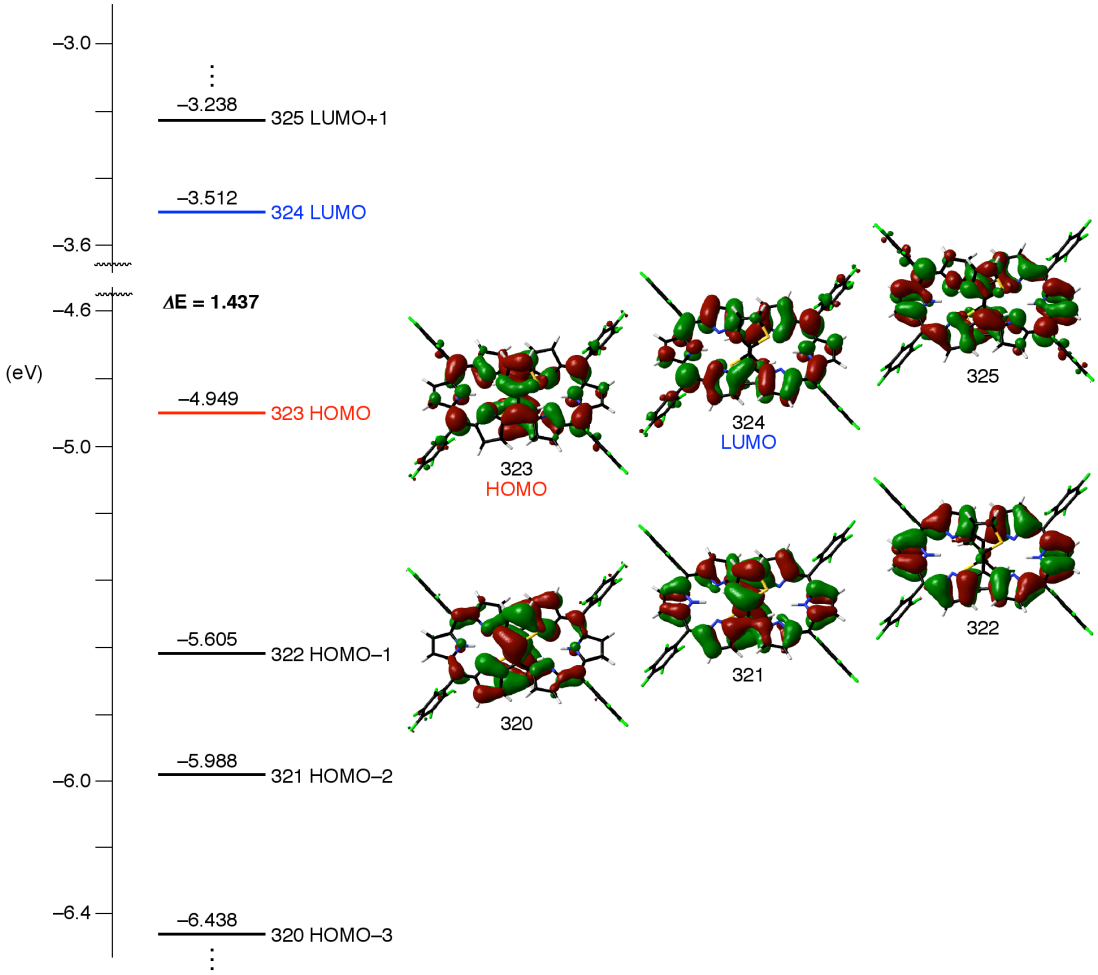

Figure S27. Frontier orbital diagrams of **T1**.

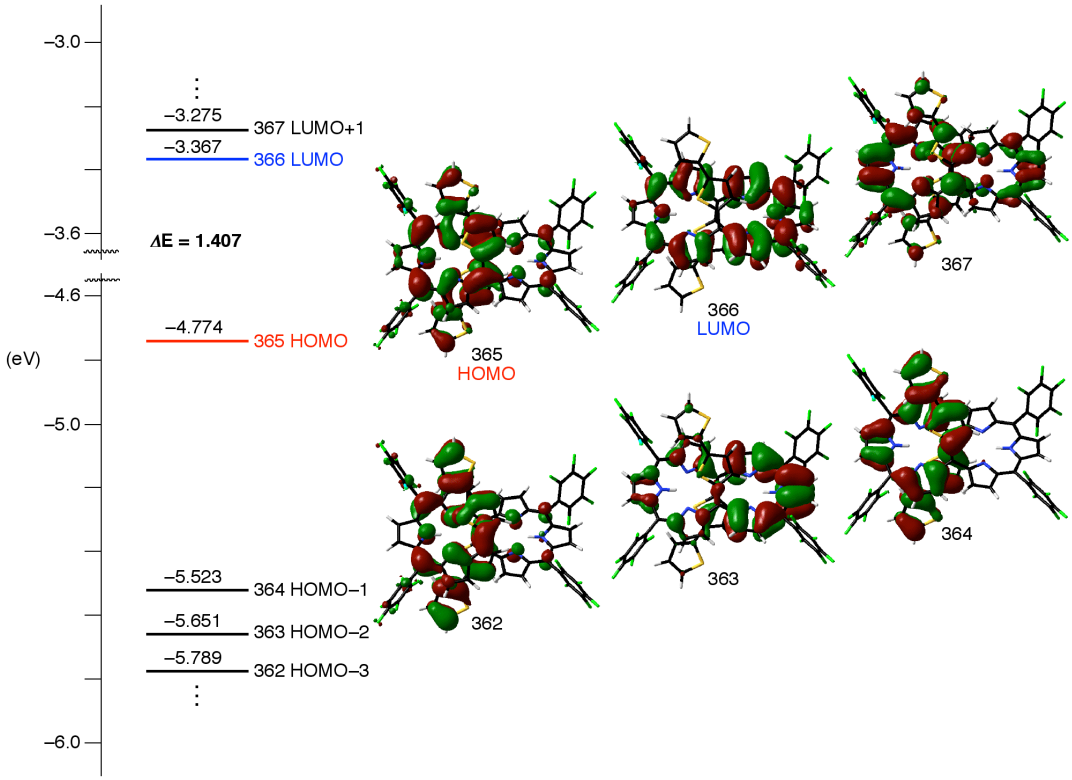

Figure S28. Frontier orbital diagrams of **T2**.

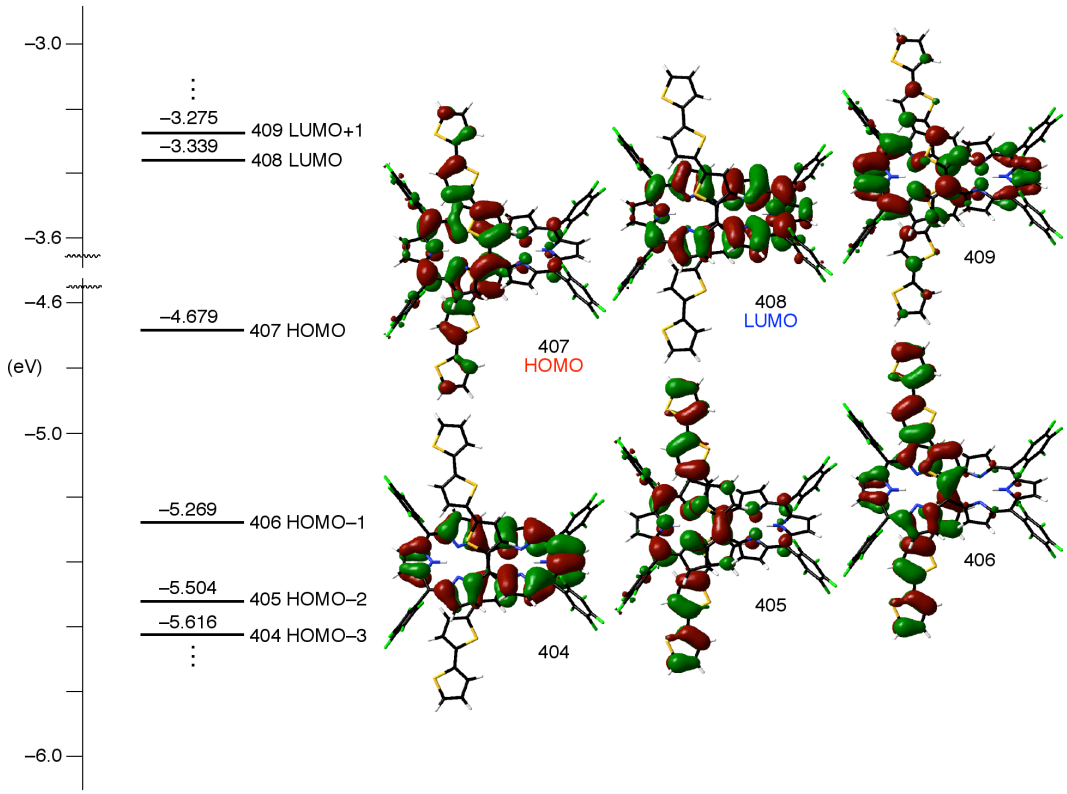

Figure S29. Frontier orbital diagrams of **T3**.

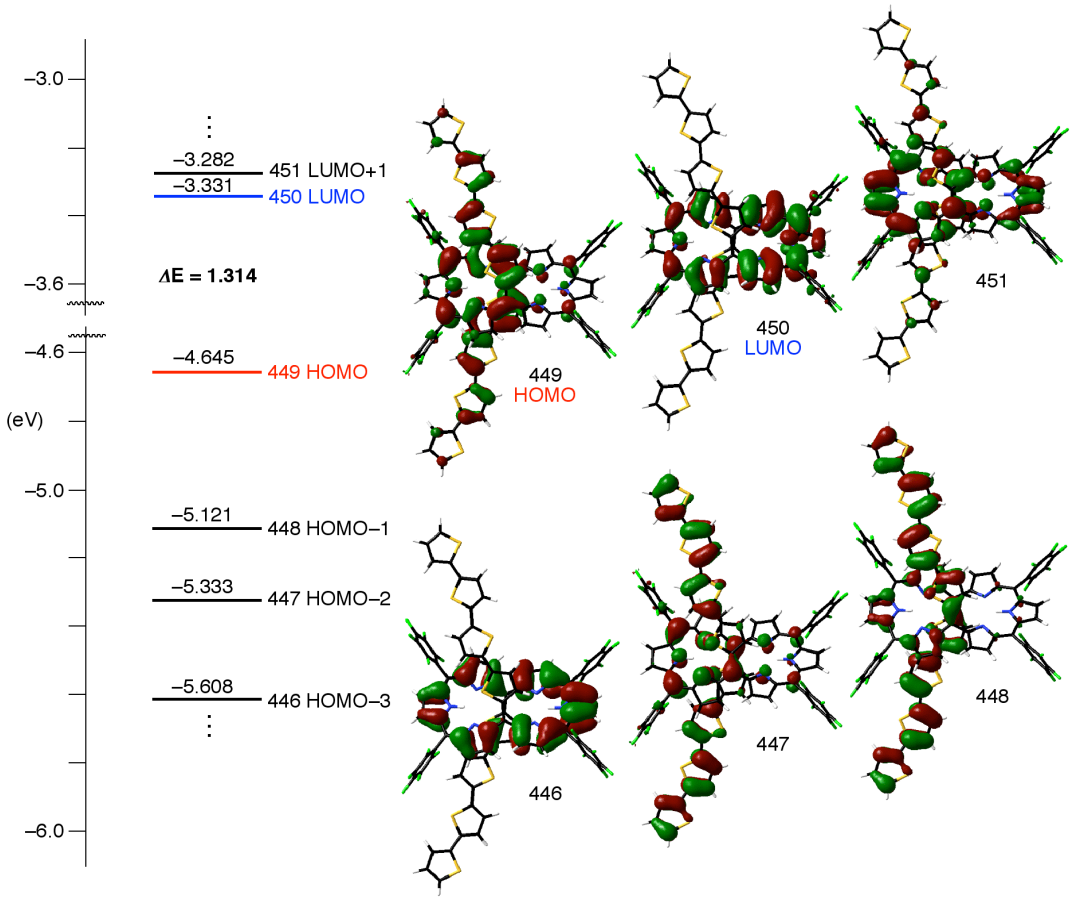

Figure S30. Frontier orbital diagrams of **T4**.

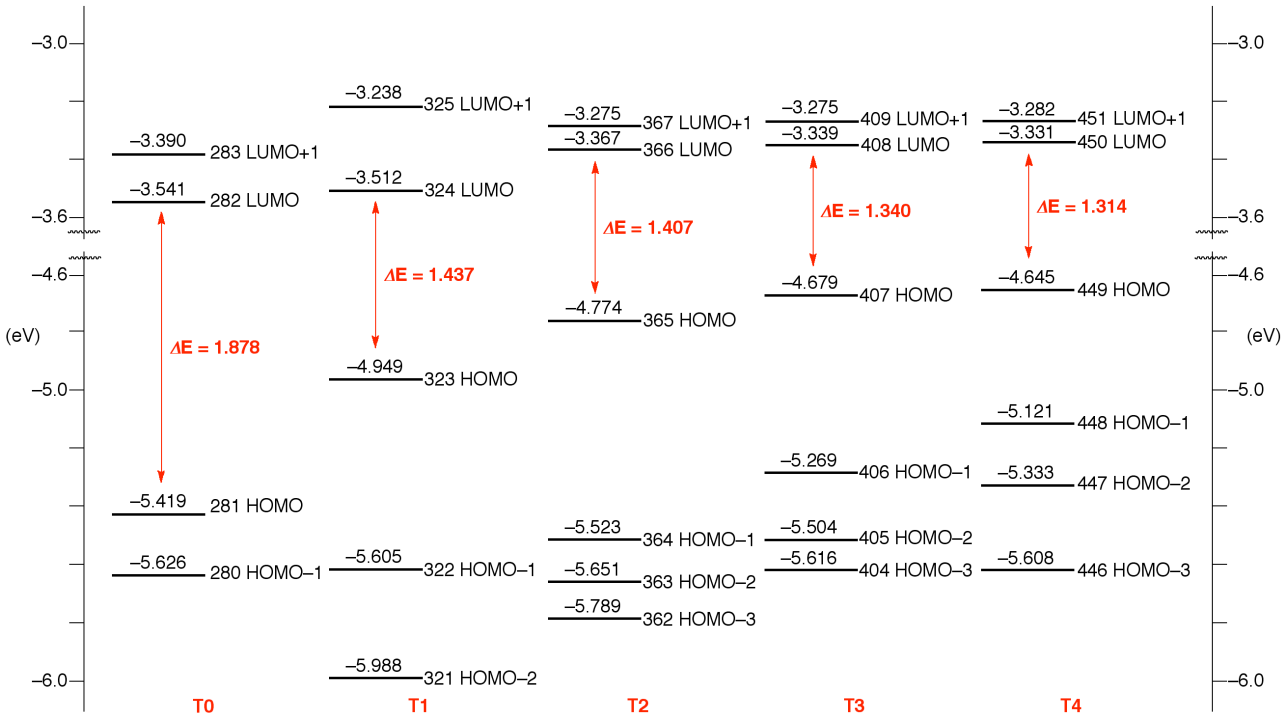

Figure S31. Summary of energy diagrams of **T0–T4**.

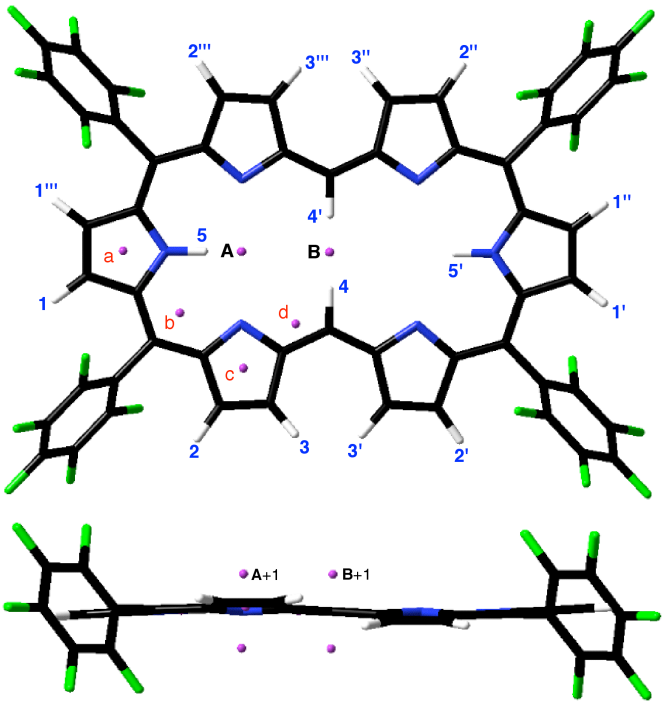

position	NICS (ppm)
a	−12.25
b	−22.63
c	+3.64
d	−26.94

position	NICS (ppm)
A	−15.54
A+1	−13.93
B	−15.00
B+1	−12.98

^{1}H	δ (ppm)
1/1'	9.55
2/2'	9.28
3/3'	10.85
4/4'	−9.34
5/5'	−6.45

Figure S32. NICS values at various positions and simulated chemical shifts of **T0**.

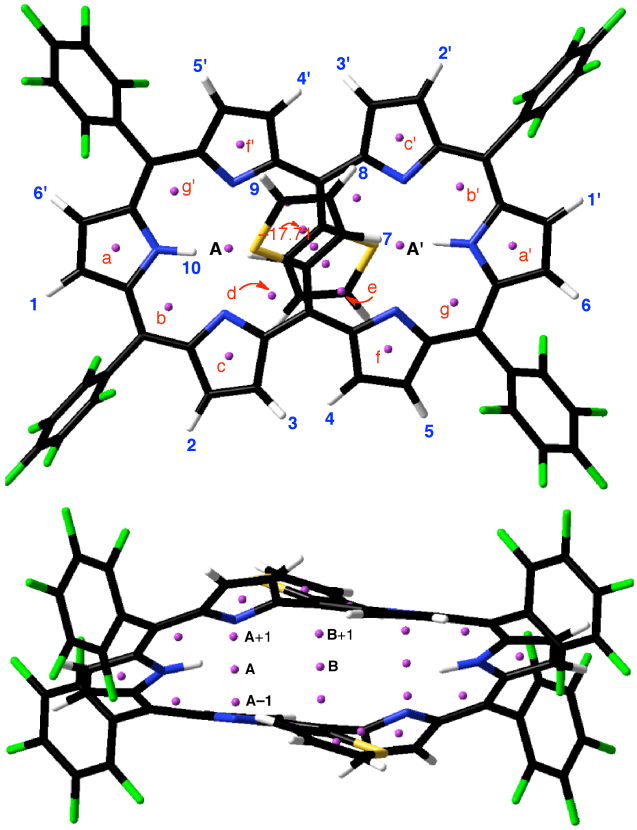

position	NICS (ppm)
a/a'	−11.30
b/b'	−17.29
c/c'	+0.96
d/d'	−7.23
e/e'	−9.90
f/f'	−1.27
g/g'	−17.48
h/h'	−17.71

position	NICS (ppm)
A	−12.21
A+1	−10.69
A−1	−11.64
B	−14.98
B+1	−25.15

^{1}H	δ (ppm)
1/1'	8.80
2/2'	9.01
3/3'	9.61
4/4'	8.97
5/5'	7.17
6/6'	8.85
7/7'	0.40
8/8'	3.10
9/9'	3.99
10/10'	−2.60

Figure S33. NICS values at various positions and simulated chemical shifts of **T1** on the optimized structure.

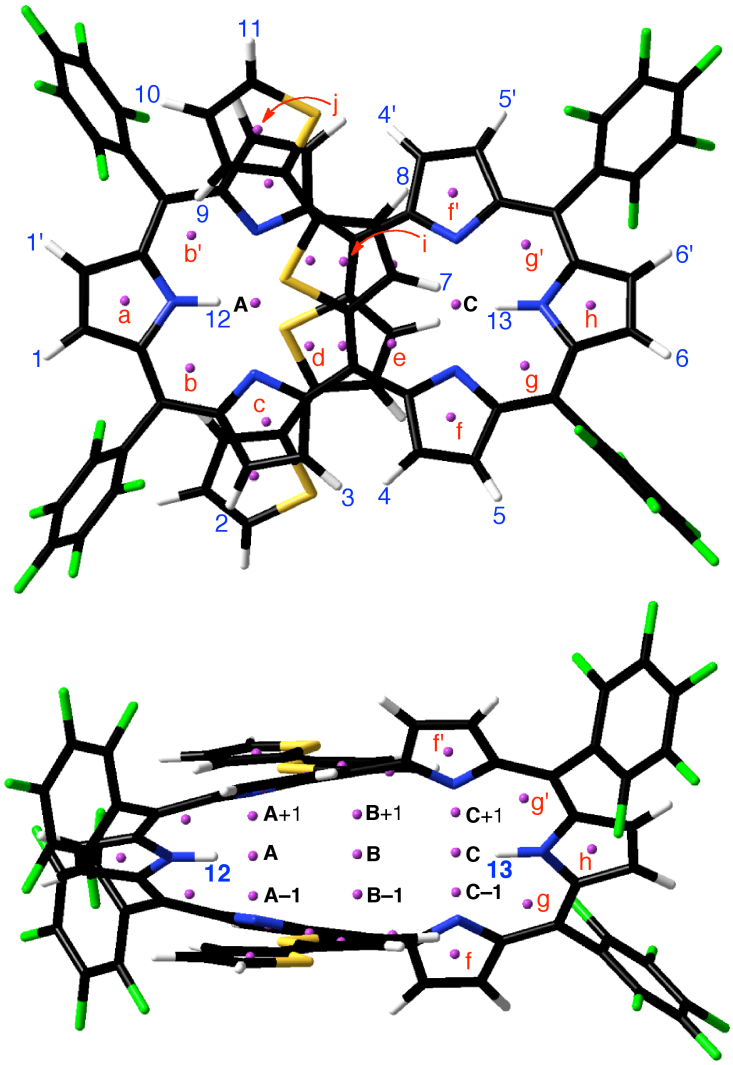

position	NICS (ppm)
a	–8.33
b/b'	–11.29 / –11.25
c/c'	+2.14 / +2.10
d/d'	–7.19 / –7.10
e/e'	–8.02 / –8.31
f/f'	+0.33 / +0.48
g/g'	–10.70 / –10.48
h	–11.64
i/i'	–12.65 / –12.74
j/j'	–12.50 / –12.49

position	NICS (ppm)
A	–8.50
A+1	–7.78
A–1	–8.01
B	–9.95
B+1	–17.00
B–1	–17.31
C	–7.21
C+1	–6.92
C–1	–7.02

^{1}H	δ (ppm)
1/1'	8.12 / 8.12
2/2'	6.05 / 6.12
3/3'	7.98 / 8.07
4/4'	8.42 / 8.37
5/5'	8.12 / 8.05
6/6'	7.82 / 7.85
7/7'	3.24 / 3.10
8/8'	4.45 / 4.44
9/9'	4.82 / 4.83
10/10'	6.16 / 6.14
11/11'	6.30 / 6.29
12/12'	2.03
13/13'	3.06

Figure S34. NICS values at various positions and simulated chemical shifts of **T2** on the optimized structure.

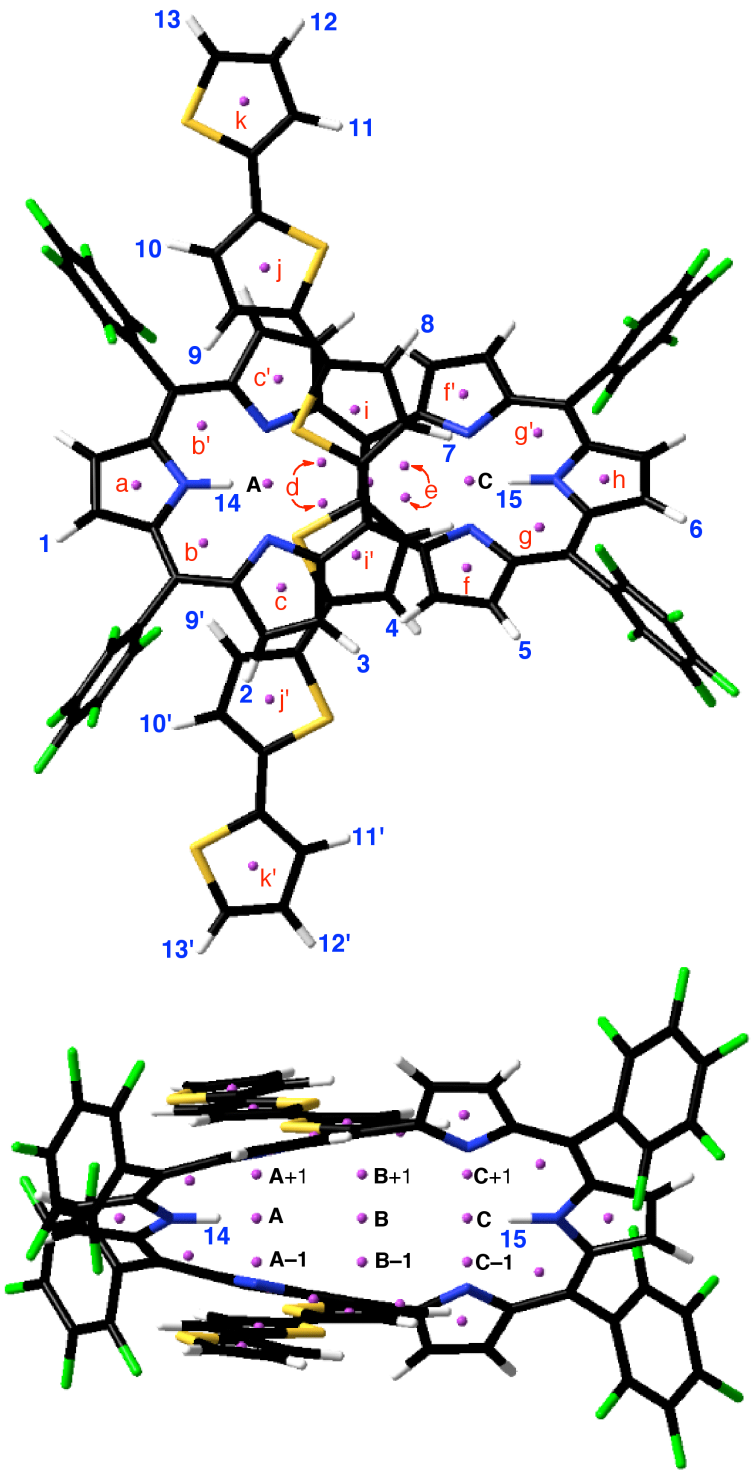

position	NICS (ppm)
a	–8.42
b/b'	–10.94
c/c'	–2.24
d/d'	–7.03
e/e'	–7.94
f/f'	+0.17
g/g'	–10.42
h	–11.51
i/i'	–12.52
j/j'	–10.64
k/k'	–11.52

position	NICS (ppm)
A	–8.30
A+1	–8.77
A–1	–8.77
B	–9.75
B+1	–16.76
B–1	–16.76
C	–7.17
C+1	–9.39
C–1	–9.39

^{1}H	δ (ppm)
1/1'	8.09
2/2'	6.09
3/3'	7.98
4/4'	8.34
5/5'	8.06
6/6'	7.79
7/7'	3.42
8/8'	4.43
9/9'	4.67
10/10'	6.31
11/11'	6.47
12/12'	6.47
13/13'	6.62
14	2.18
15	3.09

Figure S35. NICS values at various positions and simulated chemical shifts of **T3** on the optimized structure.

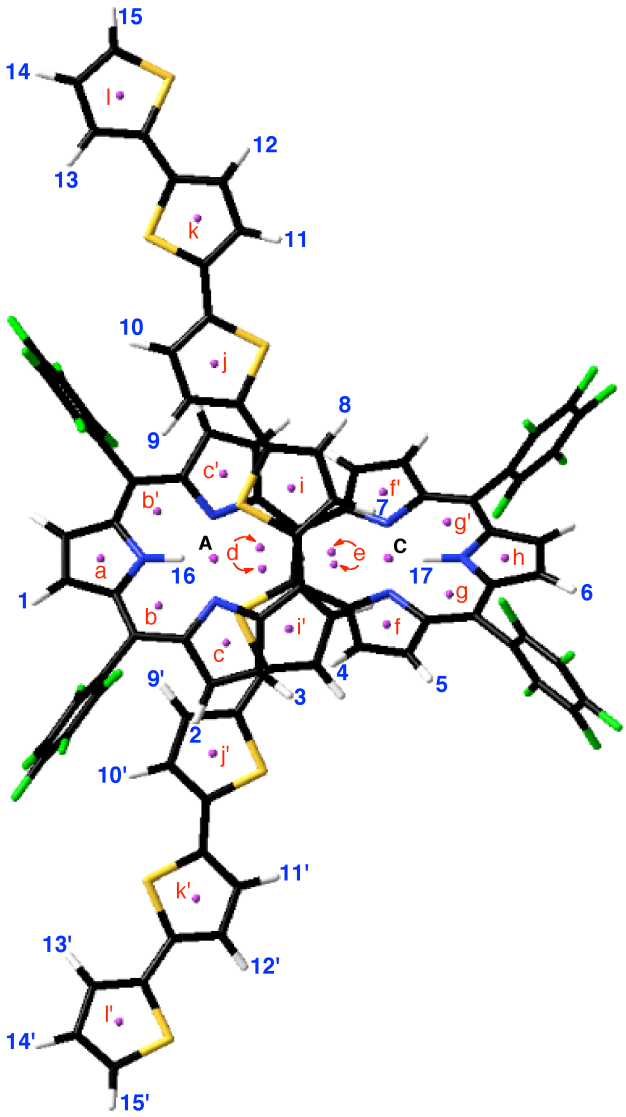

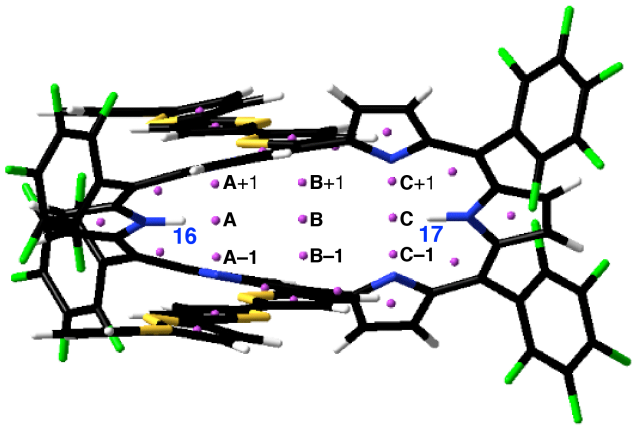

position	NICS (ppm)
a	–8.45
b/b'	–10.90
c/c'	–2.26
d/d'	–7.04
e/e'	–7.80
f/f'	–0.15
g/g'	–10.41
h	–11.52
i/i'	–12.47
j/j'	–10.66
k/k'	–9.84
l/l'	–11.63

^{1}H	δ (ppm)
1/1'	8.08
2/2'	6.07
3/3'	7.96
4/4'	8.31
5/5'	8.06
6/6'	7.77
7/7'	3.47
8/8'	4.45
9/9'	4.71
10/10'	6.14
11/11'	6.28
12/12'	6.51
13/13'	6.83
14/14'	6.69
15/15'	6.74
16	2.24
17	3.15

position	NICS (ppm)
A	–8.23
A+1	–9.63
A–1	–9.63
B	–9.73
B+1	–16.65
B–1	–16.65
C	–7.13
C+1	–10.67
C–1	–10.67

Figure S36. NICS values at various positions and simulated chemical shifts of **T4** on the optimized structure.

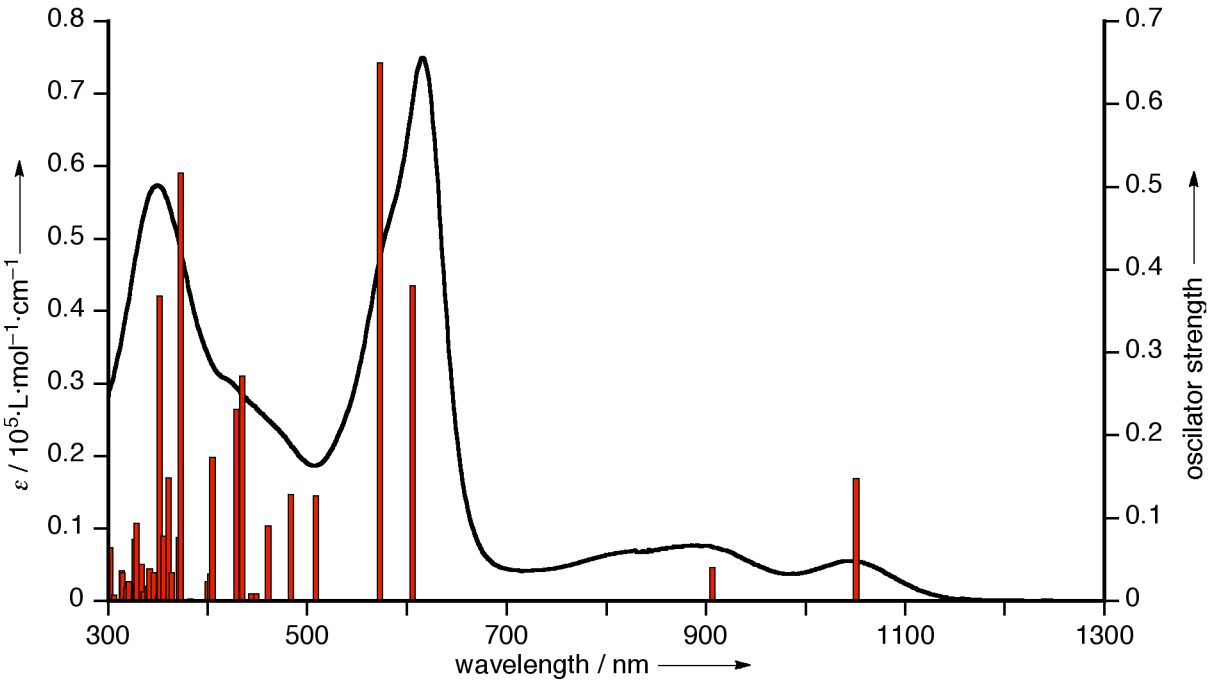

λ (nm)	*f*	λ (nm)	*f*	λ (nm)	*f*
1050.30	0.1492	382.15	0.0032	335.76	0.0117
906.31	0.0413	376.58	0.0006	333.76	0.0449
605.98	0.3817	372.42	0.5178	328.78	0.0947
572.10	0.6506	370.75	0.0776	327.63	0.0221
508.72	0.1278	363.03	0.0340	326.47	0.0752
483.73	0.1293	360.31	0.1498	320.29	0.0245
460.90	0.0914	355.09	0.0786	318.53	0.0174
448.23	0.0092	351.63	0.3691	317.42	0.0055
443.03	0.0093	350.25	0.0078	316.79	0.0010
434.62	0.2726	349.27	0.0048	314.12	0.0352
428.61	0.2324	345.02	0.0349	313.22	0.0378
404.41	0.1740	341.74	0.0397	305.51	0.0082
402.70	0.0336	339.28	0.0187	301.04	0.0652
399.58	0.0244				

Figure S37. Calculated absorption spectra on the basis of optimized structures (bars) and observed absorption spectra (lines) of **T1**.

Table S2. The detailed information about TD-DFT calculation of **T1**. (Excited state 1–15)

Excited State 1: 1050.25 nm, f=0.1492

322 -> 324	0.15587
322 -> 325	-0.22360
323 -> 324	0.63636 (HOMO to LUMO)
323 -> 325	0.15862

Excited State 2: 906.31 nm, f=0.0413

322 -> 324	0.30353
323 -> 324	-0.21412
323 -> 325	0.60341 (HOMO to LUMO+1)

Excited State 3: 623.39 nm, f=0.0000

321 -> 324	0.61958 (HOMO–2 to LUMO)
323 -> 326	0.33174

Excited State 4: 605.98 nm, f=0.3817

322 -> 324	0.59761 (HOMO–1 to LUMO)
322 -> 325	0.15099
323 -> 325	-0.33096
323 <- 325	0.11510

Excited State 5: 577.37 nm, f=0.0000

319 -> 324	-0.11339
321 -> 324	-0.26836
321 -> 325	-0.41781
323 -> 326	0.44005 (HOMO to LUMO+2)
323 -> 327	-0.18796

Excited State 6: 572.10 nm, f=0.6506

318 -> 324	-0.10633
320 -> 324	-0.25811
322 -> 324	-0.13603
322 -> 325	0.58596 (HOMO–1 to LUMO+1)
323 -> 324	0.21040
323 -> 325	0.10320

Excited State 7: 523.36 nm, f=0.0000

319 -> 324	-0.11230
321 -> 324	-0.14005
321 -> 325	0.31043
323 -> 326	0.35168
323 -> 327	0.46922 (HOMO to LUMO+3)

Excited State 8: 508.72 nm, f=0.1278

314 -> 324	0.10852
318 -> 324	-0.28879
320 -> 324	0.58435 (HOMO–3 to LUMO)
322 -> 325	0.17473
323 -> 328	0.11325

Excited State 9: 500.47 nm, f=0.0000

316 -> 324	-0.14799
317 -> 324	-0.12866
321 -> 325	-0.42930
322 -> 326	0.20272
323 -> 326	-0.17250
323 -> 327	0.43072 (HOMO to LUMO+3)

Excited State 10: 487.78 nm, f=0.0000

317 -> 324	0.24306
319 -> 324	0.62266 (HOMO–4 to LUMO)
319 -> 325	0.13079

Excited State 11: 483.73 nm f=0.1293

314 -> 324	0.16781
318 -> 324	0.60043 (HOMO–5 to LUMO)
320 -> 324	0.19430
320 -> 325	-0.11583
322 -> 325	0.13476
323 -> 328	0.16714

Excited State 12: 474.26 nm, f=0.0000

317 -> 324	0.64118 (HOMO–6 to LUMO)
319 -> 324	-0.21206
321 -> 325	-0.10008
323 -> 326	-0.14567

Excited State 13: 460.90 nm. f=0.0914

314 -> 324	0.17444
318 -> 324	0.13355
318 -> 325	-0.14536
320 -> 325	0.55768 (HOMO–3 to LUMO+1)
323 -> 328	-0.31740

Excited State 14: 455.27 nm, f=0.0000

313 -> 324	0.25489
316 -> 324	0.61709 (HOMO–7 to LUMO)
322 -> 326	0.17202

Excited State 15: 448.23 nm, f=0.0092

314 -> 324	0.21670
315 -> 324	0.61437 (HOMO–7 to LUMO)
320 -> 325	-0.16255
323 -> 328	-0.16068

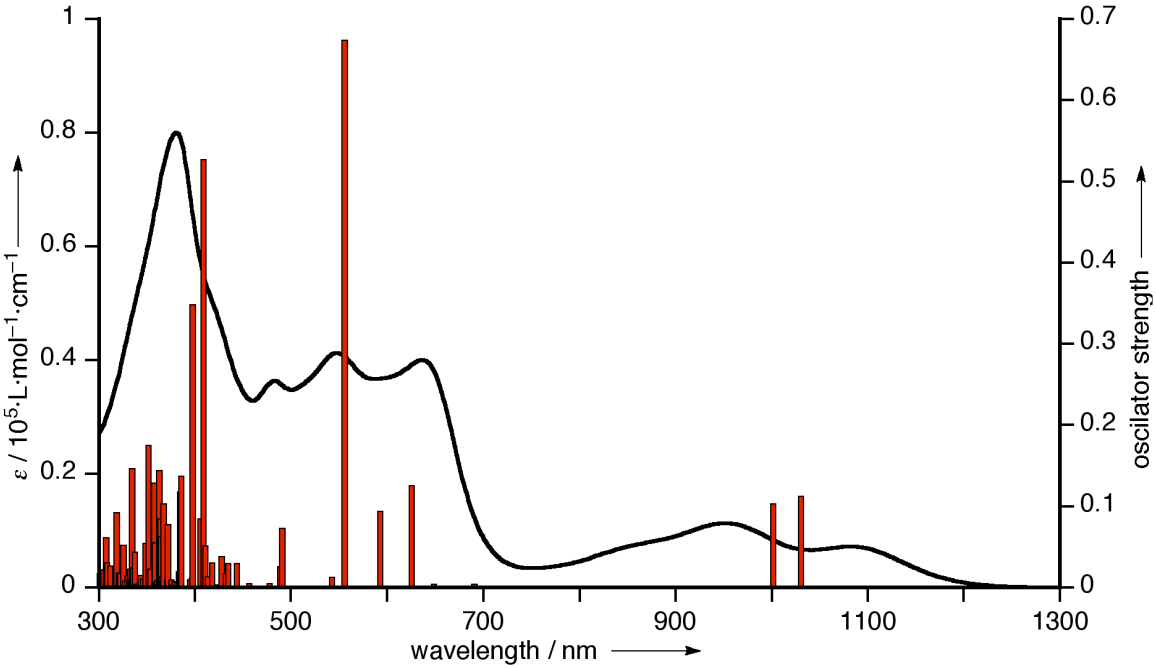

λ (nm)	*f*	λ (nm)	*f*	λ (nm)	*f*	λ (nm)	*f*
1130.70	0.1137	408.23	0.5279	359.78	0.0072	325.82	0.0525
1002.00	0.1039	405.22	0.0858	358.87	0.0558	324.13	0.0013
724.03	0.0001	397.79	0.3488	357.22	0.1298	321.93	0.0184
690.74	0.0051	396.04	0.0124	357.16	0.0051	321.73	0.0175
648.64	0.0048	394.29	0.0106	353.75	0.0237	321.38	0.0191
625.44	0.1261	385.96	0.1380	353.14	0.0022	318.01	0.0932
592.35	0.0398	384.25	0.1184	351.45	0.1758	317.07	0.0057
568.90	0.0945	383.18	0.0204	348.11	0.0550	314.76	0.0022
555.37	0.6748	381.05	0.0075	345.74	0.0111	311.96	0.0278
542.03	0.0133	378.50	0.0083	344.63	0.0007	308.88	0.0313
490.32	0.0736	377.69	0.0039	344.12	0.0159	307.08	0.0622
488.05	0.0262	375.88	0.0104	343.61	0.0001	304.46	0.0227
477.87	0.0058	374.27	0.0015	340.71	0.0034	304.00	0.0125
456.10	0.0057	371.28	0.0782	338.37	0.0044	302.84	0.0213
443.03	0.0220	371.11	0.0352	337.17	0.0445	302.38	0.0110
434.33	0.0300	370.18	0.0103	335.87	0.0248	302.18	0.0023
434.03	0.0689	367.93	0.1041	334.82	0.1472	300.46	0.0181
431.59	0.0033	367.55	0.0099	333.98	0.0108	300.26	0.0132
431.36	0.0184	367.24	0.0143	333.66	0.0013		
427.35	0.0388	366.12	0.0639	332.39	0.0231		
426.31	0.0012	364.76	0.0852	332.13	0.0110		
424.37	0.0042	364.48	0.1445	329.41	0.0148		
417.88	0.0308	361.99	0.0040	328.54	0.0010		
413.16	0.0143	361.78	0.0094	327.88	0.0001		
410.39	0.0517	360.88	0.0025	327.24	0.0088		

Figure S38. Calculated absorption spectra on the basis of optimized structures (bars) and observed absorption spectra (lines) of **T2**.

Table S3. The detailed information about TD-DFT calculation of **T2**. (Excited state 1–15)

Excited State 1: 1130.66 nm, f=0.1137

363 -> 367	0.14821
364 -> 367	-0.10000
365 -> 366	0.68345 (HOMO to LUMO)

Excited State 2: 1001.95 nm, f=0.1039

363 -> 366	-0.14184
365 -> 367	0.69778 (HOMO to LUMO+1)

Excited State 3: 724.03 nm, f=0.0001

363 -> 366	0.10523
364 -> 366	0.69123 (HOMO–1 to LUMO)

Excited State 4: 690.74 nm, f=0.0051

362 -> 366	-0.15966
364 -> 367	0.53085 (HOMO–1 to LUMO+1)
365 -> 368	-0.43096

Excited State 5: 648.64 nm, f=0.0048

362 -> 366	0.54476 (HOMO–3 to LUMO)
363 -> 367	0.42358
365 -> 368	-0.12491

Excited State 6: 625.44 nm, f=0.1261

362 -> 367	-0.43985
363 -> 366	0.51205 (HOMO–2 to LUMO)
365 -> 367	0.12797
365 -> 369	-0.15061

Excited State 7: 592.35 nm, f=0.0398

362 -> 366	-0.13404
363 -> 367	0.27673
364 -> 367	0.37122
365 -> 368	0.51243 (HOMO to LUMO+2)

Excited State 8: 568.90 nm, f=0.0945

362 -> 367	0.46103 (HOMO–3 to LUMO+1)
363 -> 366	0.38912
364 -> 368	0.14497
365 -> 370	0.29590

Excited State 9: 555.37 nm, f=0.6748

362 -> 366	-0.38012
363 -> 367	0.46031 (HOMO–2 to LUMO+1)
364 -> 367	-0.25468
365 -> 366	-0.17063
365 -> 368	-0.17134

Excited State 10: 542.03 nm, f=0.0133

362 -> 367	-0.10545
363 -> 368	0.11020
364 -> 368	-0.11221
365 -> 369	0.66605 (HOMO to LUMO+4)

Excited State 11: 2.5287 eV, 490.32 nm f=0.0736

361 -> 366	0.39049
364 -> 368	-0.31401
365 -> 370	0.47796 (HOMO to LUMO+5)

Excited State 12: 488.05 nm, f=0.0262

361 -> 366	0.57652 (HOMO–4 to LUMO)
364 -> 368	0.26694
365 -> 370	-0.26729

Excited State 13: 477.87 nm, f=0.0058

361 -> 367	0.69074 (HOMO–4 to LUMO+1)

Excited State 14: 456.10 nm, f=0.0057

355 -> 366	0.14640
356 -> 366	0.12087
360 -> 366	0.63989 (HOMO–5 to LUMO)
363 -> 368	0.16038

Excited State 15: 443.03 nm, f=0.0220

354 -> 366	-0.12130
357 -> 366	-0.24470
359 -> 366	0.60275 (HOMO–6 to LUMO)
362 -> 368	-0.18632

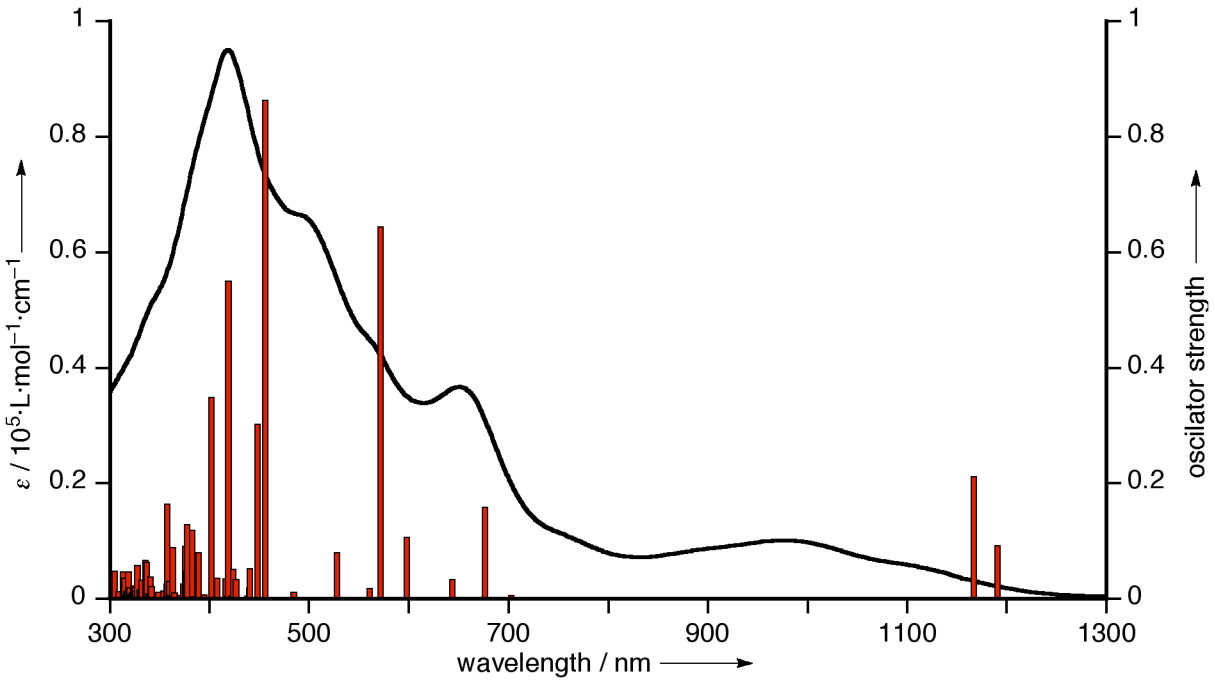

λ (nm)	*f*	λ (nm)	*f*	λ (nm)	*f*	λ (nm)	*f*
1190.90	0.0938	418.28	0.0057	359.83	0.0004	332.17	0.0329
1066.70	0.2131	415.31	0.0360	359.04	0.0321	330.69	0.0168
804.41	0.0018	411.21	0.0012	358.26	0.0043	330.44	0.0168
754.76	0.0002	407.79	0.0366	357.40	0.1650	327.95	0.0588
702.86	0.0073	405.10	0.0041	356.95	0.0269	326.43	0.0027
676.04	0.1589	401.72	0.3491	355.19	0.0021	326.40	0.0153
643.17	0.0344	400.35	0.0252	353.21	0.0149	325.91	0.0197
597.57	0.1075	394.99	0.0785	352.77	0.0193	325.28	0.0231
571.13	0.6455	388.12	0.0809	351.53	0.0031	324.58	0.0081
560.05	0.0186	383.63	0.0050	350.93	0.0008	323.29	0.0024
527.23	0.0816	383.16	0.1195	349.46	0.0035	322.62	0.0114
497.14	0.0120	377.08	0.1298	348.90	0.0125	321.01	0.0014
491.96	0.0005	376.71	0.0477	346.26	0.0054	320.62	0.0088
484.97	0.0125	376.13	0.0918	346.19	0.0042	320.44	0.0199
471.44	0.0045	374.63	0.0003	345.74	0.0005	319.17	0.0476
462.60	0.0007	373.26	0.0270	345.28	0.0021	318.88	0.0134
456.45	0.0044	369.67	0.0071	341.84	0.0227	317.89	0.0127
455.61	0.8646	369.25	0.0012	341.47	0.0083	317.32	0.0075
447.18	0.3029	367.97	0.0045	340.20	0.0394	314.08	0.0363
440.51	0.0536	366.87	0.0042	339.67	0.0105	313.30	0.0093
439.54	0.0200	366.57	0.0001	338.77	0.0093	312.06	0.0476
437.82	0.0525	366.40	0.0031	338.24	0.0024	310.29	0.0014
428.06	0.0033	365.21	0.0115	336.81	0.0641	310.17	0.0030
426.33	0.0351	364.52	0.0468	335.01	0.0677	308.78	0.0135
423.22	0.0525	364.49	0.0893	333.41	0.0004	304.11	0.0490
421.70	0.0062	363.98	0.0191	332.86	0.0017	302.97	0.0012
418.95	0.5506	361.54	0.0067	332.48	0.0015	301.91	0.0057
						301.35	0.0040
						301.10	0.0029
						300.02	0.0121

Figure S39. Calculated absorption spectra on the basis of optimized structures (bars) and observed absorption spectra (lines) of **T3**.

Table S4. The detailed information about TD-DFT calculation of **T3**. (Excited state 1–15)

Excited State 1: 1190.95 nm, f=0.0938

404 -> 409	0.14645	
407 -> 408	0.68845	(HOMO to LUMO)

Excited State 2: 1066.72 nm, f=0.2131

404 -> 408	-0.11374	
407 -> 409	0.70413	(HOMO to LUMO+1)

Excited State 3: 804.41 nm, f=0.0018

406 -> 408	0.70177	(HOMO–1 to LUMO)

Excited State 4: 754.76 nm, f=0.0002

405 -> 408	-0.13966	
406 -> 409	0.59806	(HOMO–1 to LUMO+1)
407 -> 410	-0.33812	

Excited State 5: 702.86 nm, f=0.0073

404 -> 409	0.33368	
405 -> 408	0.60254	(HOMO–2 to LUMO)
406 -> 409	0.11832	

Excited State 6: 676.04 nm, f=0.1589

404 -> 408	-0.34311	
405 -> 409	0.59554	(HOMO–2 to LUMO+1)
407 -> 411	-0.10428	

Excited State 7: 643.17 nm, f=0.0344

404 -> 409	0.13534	
406 -> 409	0.33885	
407 -> 410	0.60134	(HOMO to LUMO+2)

Excited State 8: 597.57 nm, f=0.1075

404 -> 408	0.52412	(HOMO–3 to LUMO)
405 -> 409	0.27346	
406 -> 410	0.18249	
407 -> 412	0.31959	

Excited State 9: 571.13 nm, f=0.6455

404 -> 409	0.58153	(HOMO–3 to LUMO+1)
405 -> 408	-0.31713	
407 -> 408	-0.15886	
407 -> 410	-0.11056	

Excited State 10: 560.05 nm, f=0.0186

404 -> 410	-0.10803	
407 -> 411	0.67222	(HOMO to LUMO+3)

Excited State 11: 527.23 nm, f=0.0816

404 -> 408	-0.10595	
405 -> 409	-0.10682	
406 -> 410	-0.44059	
407 -> 412	0.51655	(HOMO to LUMO+4)

Excited State 12: 497.14 nm, f=0.0120

402 -> 408	-0.16725	
403 -> 408	0.65621	(HOMO–4 to LUMO)
404 -> 410	-0.12639	

Excited State 13: 491.96 nm, f=0.0005

402 -> 409	-0.32863	
403 -> 409	0.57675	(HOMO–4 to LUMO+1)
405 -> 410	0.18386	

Excited State 14: 484.97 nm, f=0.0125

401 -> 409	0.10316	
402 -> 408	0.66732	(HOMO–5 to LUMO)
403 -> 408	0.14590	

Excited State 15: 471.44 nm, f=0.0045

402 -> 409	0.57929	(HOMO–5 to LUMO+1)
403 -> 409	0.21149	
405 -> 410	0.32146	

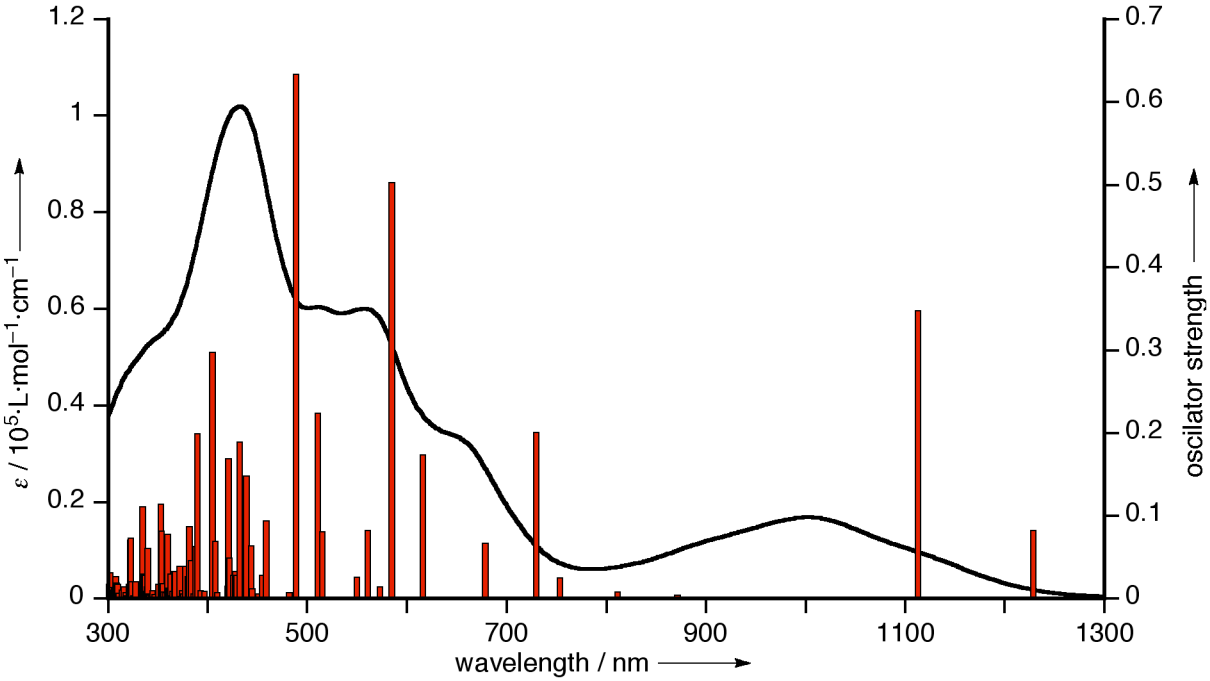

λ (nm)	*f*	λ (nm)	*f*	λ (nm)	*f*	λ (nm)	*f*
1228.40	0.0827	420.29	0.1695	360.89	0.0135	331.22	0.0031
1113.00	0.3492	419.79	0.0158	360.52	0.0786	327.89	0.0209
871.20	0.0046	414.66	0.0002	359.04	0.0028	325.21	0.0038
811.40	0.0090	409.55	0.0084	358.11	0.0085	324.19	0.0023
753.61	0.0253	407.05	0.0699	355.35	0.0088	323.82	0.0209
729.51	0.2015	404.38	0.2981	355.22	0.0193	323.43	0.0740
678.45	0.0680	397.66	0.0005	354.74	0.0004	322.32	0.0716
615.64	0.1748	396.84	0.0096	353.43	0.0824	321.45	0.0179
584.17	0.5041	392.97	0.0105	353.26	0.0005	321.10	0.0006
572.54	0.0152	389.07	0.1998	353.01	0.1147	319.49	0.0010
560.03	0.0830	387.97	0.0636	350.54	0.0177	319.16	0.0006
549.88	0.0269	385.58	0.0061	346.18	0.0054	318.80	0.0043
545.20	0.0013	383.65	0.0472	344.82	0.0100	318.63	0.0085
514.67	0.0816	381.30	0.0874	344.63	0.0037	316.03	0.0070
510.42	0.2247	379.24	0.0271	342.37	0.0016	315.49	0.0149
498.61	0.0020	377.56	0.0399	341.95	0.0045	313.96	0.0114
488.41	0.6344	375.96	0.0064	341.71	0.0060	310.17	0.0073
481.12	0.0018	375.80	0.0102	340.61	0.0002	309.26	0.0178
477.09	1.2269	374.24	0.0006	340.41	0.0042	308.39	0.0198
470.77	0.0001	372.90	0.0033	339.71	0.0614	308.17	0.0277
458.23	0.0948	371.16	0.0396	339.60	0.0021	306.34	0.0117
454.44	0.0288	368.30	0.0010	339.29	0.0147	305.58	0.0135
450.73	0.0060	367.77	0.0010	339.28	0.0037	303.96	0.0113
444.98	0.0126	367.59	0.0337	338.30	0.0096	303.63	0.0015
443.23	0.0641	366.37	0.0331	337.63	0.0285	302.80	0.0010
438.60	0.1484	365.39	0.0020	336.65	0.0009	302.71	0.0004
431.29	0.1903	364.81	0.0096	336.39	0.0308	302.58	0.0066
428.42	0.0292	364.79	0.0040	336.17	0.0003	301.52	0.0138
427.00	0.0332	364.03	0.0309	334.71	0.1113	301.12	0.0321
425.50	0.0288	362.78	0.0122	333.62	0.0018	300.11	0.0178
421.07	0.0498	362.34	0.0028	332.52	0.0002		

Figure S40. Calculated absorption spectra on the basis of optimized structures (bars) and observed absorption spectra (lines) of **T4**.

Table S5. The detailed information about TD-DFT calculation of **T4**. (Excited state 1–15)

Excited State 1: 1228.40 nm, f=0.0827

446 -> 451	0.13890
449 -> 450	0.69091 (HOMO to LUMO)

Excited State 2: 1112.96 nm, f=0.3492

449 -> 451	0.70571 (HOMO to LUMO+1)

Excited State 3: 871.20 nm, f=0.0046

448 -> 450	0.70072 (HOMO–1 to LUMO)

Excited State 4: 811.40 nm, f=0.0090

447 -> 450	0.12936
448 -> 451	0.64119 (HOMO–1 to LUMO+1)
449 -> 452	-0.24789

Excited State 5: 753.61 nm, f=0.0253

446 -> 451	0.27722
447 -> 450	0.63022 (HOMO–2 to LUMO)
448 -> 451	-0.12555

Excited State 6: 729.51 nm, f=0.2015

446 -> 450	-0.24779
447 -> 451	0.64460 (HOMO–2 to LUMO+1)

Excited State 7: 678.45 nm, f=0.0680

446 -> 451	-0.10292
448 -> 451	0.25739
449 -> 452	0.64310 (HOMO to LUMO+2)

Excited State 8: 615.64 nm, f=0.1748

446 -> 450	0.54796 (HOMO–3 to LUMO)
447 -> 451	0.17120
448 -> 452	0.18832
449 -> 454	-0.33769

Excited State 9: 584.17 nm, f=0.5041

444 -> 450	0.12215
446 -> 451	0.60425 (HOMO–3 to LUMO+1)
447 -> 450	-0.27592
449 -> 450	-0.13578

Excited State 10: 572.54 nm, f=0.0152

445 -> 450	0.27878
448 -> 452	0.16632
449 -> 453	0.60671 (HOMO to LUMO+3)

Excited State 11: 560.03 nm, f=0.0830

445 -> 450	-0.41358
448 -> 452	0.31855
449 -> 453	0.13221
449 -> 454	0.42213 (HOMO to LUMO+4)

Excited State 12: 549.88 nm, f=0.0269

445 -> 450	0.46693 (HOMO–4 to LUMO)
446 -> 450	0.14042
448 -> 452	0.28634
449 -> 453	-0.24755
449 -> 454	0.30730

Excited State 13: 545.20 nm, f=0.0013

445 -> 451	0.65190 (HOMO–4 to LUMO+1)
447 -> 452	0.15495
449 -> 455	-0.13363

Excited State 14: 514.67 nm, f=0.0816

444 -> 450	0.67421 (HOMO–5 to LUMO)
446 -> 451	-0.11863

Excited State 15: 510.42 nm, f=0.2247

444 -> 451	0.58483 (HOMO–5 to LUMO+1)
447 -> 451	-0.13350
448 -> 452	0.28168
449 -> 454	-0.10801
449 -> 456	-0.10527

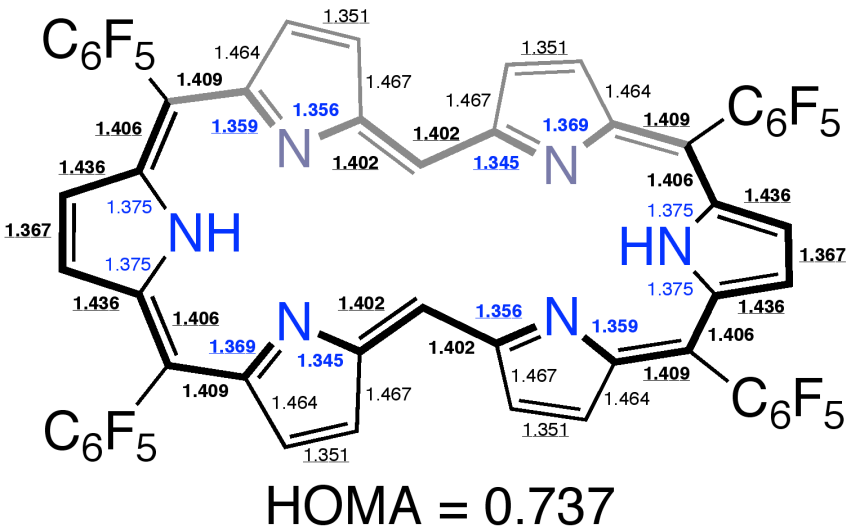

Figure S41. Selected bond length and HOMA value of **T0** on the optimized structure.

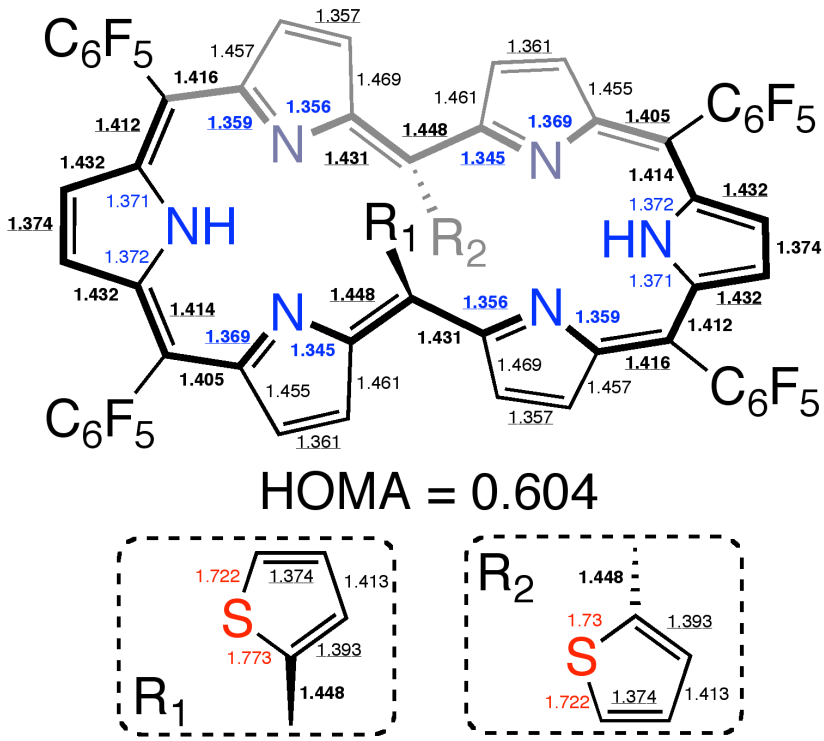

Figure S42. Selected bond length and HOMA value of **T1** on the optimized structure. The tripyrrodimethene unit on the left half is included in the helical structure.

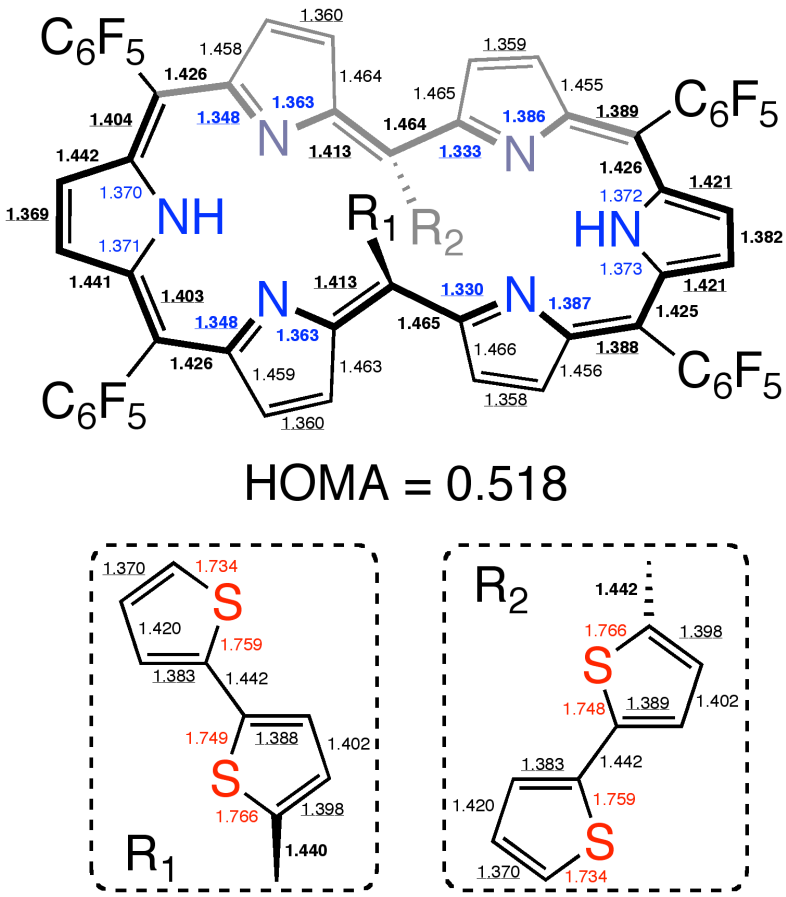

Figure S43. Selected bond length and HOMA value of **T2** on the optimized structure. The tripyrrodimethene unit on the left half is included in the helical structure.

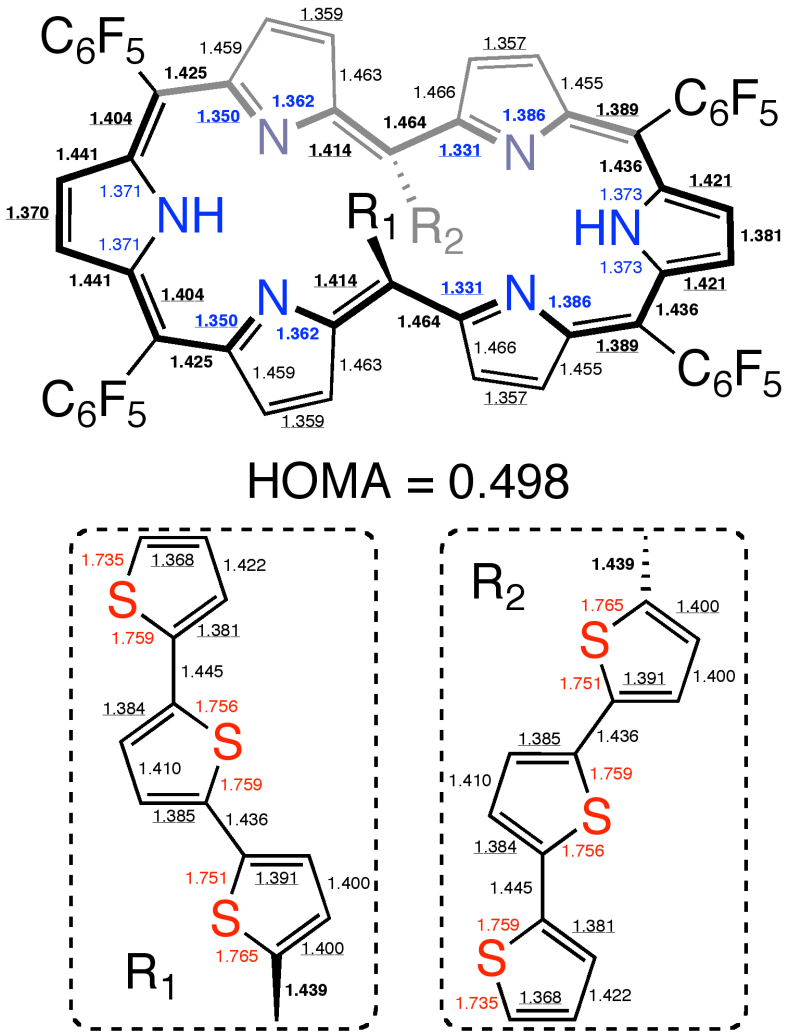

Figure S44. Selected bond length and HOMA value of **T1** on the optimized structure. The tripyrrodimethene unit on the left half is included in the helical structure.

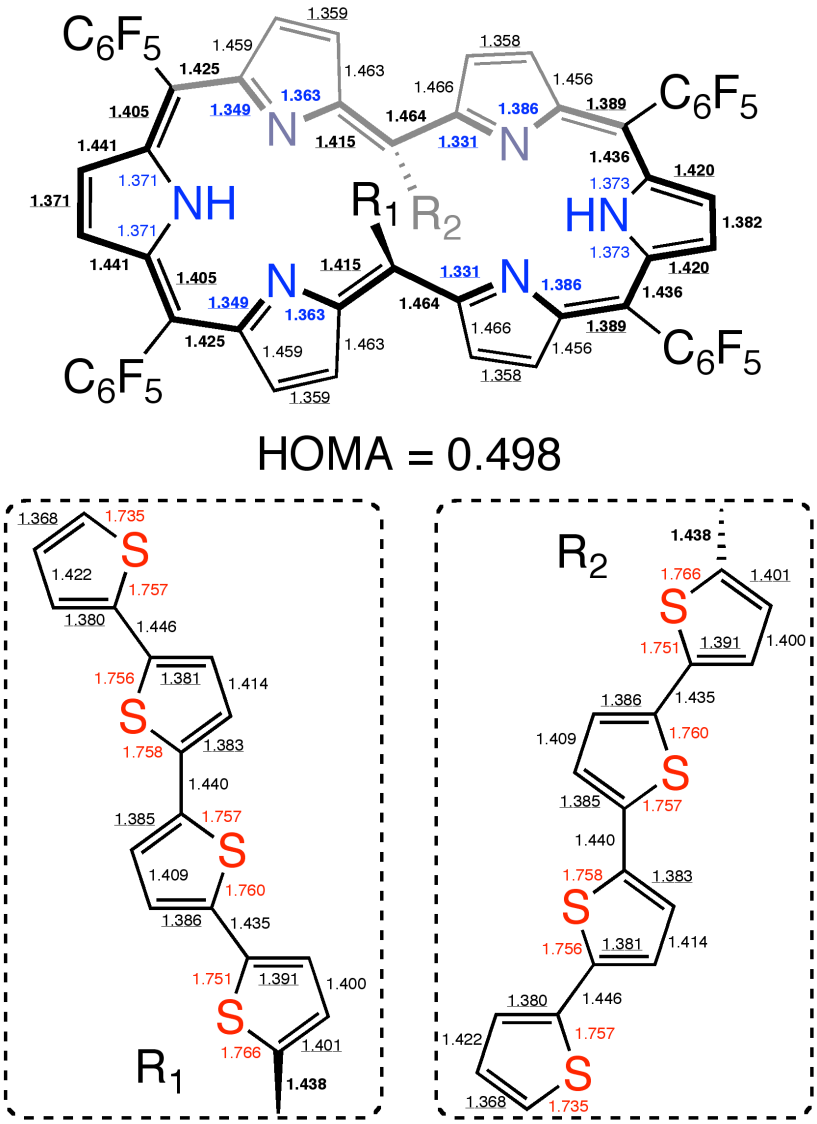

Figure S45. Selected bond length and HOMA value of **T4** on the optimized structure. The tripyrrodimethene unit on the left half is included in the helical structure.

Table S3. Summary of various spectral and photophysical data for **T0**–**T4**.

	T0	**T1**	**T2**	**T3**	**T4**
NICS (calcd.)	–15.54	–12.21	–8.50 (–7.21)	–8.30 (–7.17)	–8.26 (–7.13)
HOMA (obsd.)	0.783	0.568	0.464 (0.425)	0.397	–[a]
HOMA (calcd.)	0.737	0.604	0.518	0.498	0.498
Excited Lifetime (ps)	138	25.4	15.2	10.0	8.5
ΔE (eV vs Fc; CV)	–	1.29	1.18	1.09	1.04
ΔE (eV; calcd.)	1.88	1.44	1.41	1.35	1.31
δ (outer β-H)	10.49–9.03	8.16–7.38	8.21–5.76	8.20–5.98	8.19–6.05
δ (inner NH)	–4.97	–	8.23, 5.12	8.35, 5.22	8.41, 5.41
δ (thienyl-H)	–	5.35–4.55	6.88–4.72	7.20–4.78	7.25–4.82

[a]: The obtained data of **T4** was not sufficient to discuss the bond length in details.

7. Femtosecond Transient Absorption Spectra and Decay Profiles

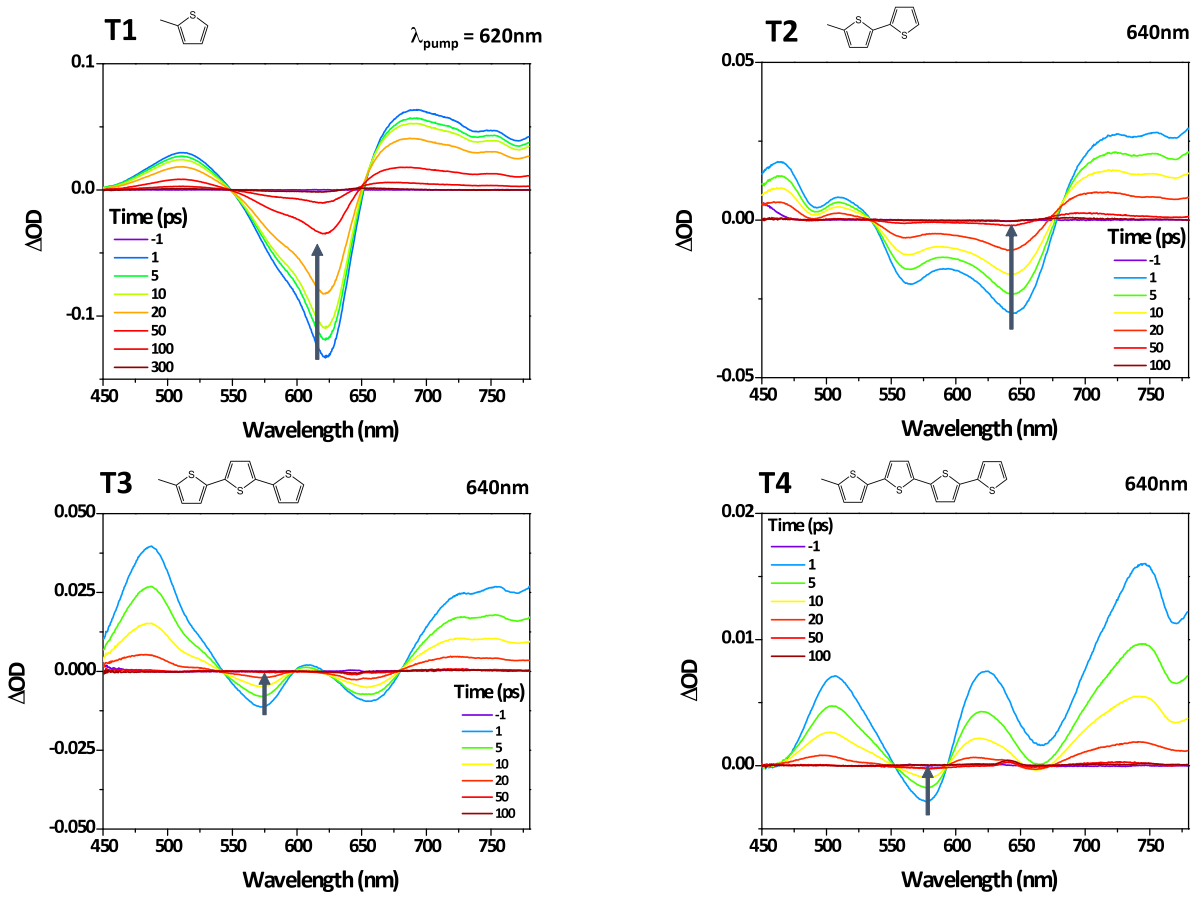

Figure S46. Femtosecond transient absorption spectra of **T1-T4** in toluene.

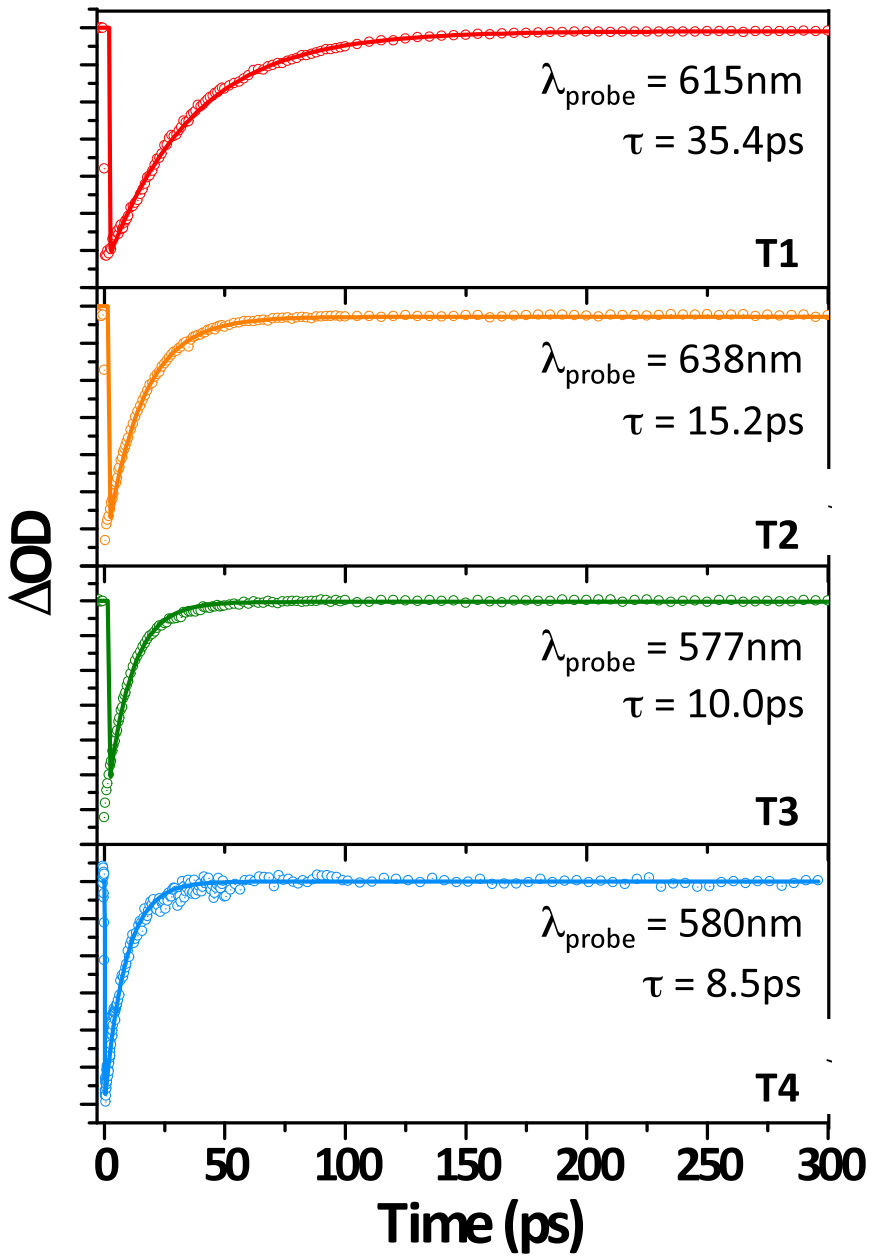

Figure S47. Decay profiles of **T1-T4**.

8. References

[S1] Gaussian 09, Revision A.02. M. J. Frisch, G. W. Trucks, H. B. Schlegel, G. E. Scuseria, M. A. Robb, J. R. Cheeseman, G. Scalmani, V. Barone, B. Mennucci, G. A. Petersson, H. Nakatsuji, M. Caricato, X. Li, H. P. Hratchian, A. F. Izmaylov, J. Bloino, G. Zheng, J. L. Sonnenberg, M. Hada, M. Ehara, K. Toyota, R. Fukuda, J. Hasegawa, M. Ishida, T. Nakajima, Y. Honda, O. Kitao, H. Nakai, T. Vreven, J. A. Montgomery, Jr., J. E. Peralta, F. Ogliaro, M. Bearpark, J. J. Heyd, E. Brothers, K. N. Kudin, V. N. Staroverov, R. Kobayashi, J. Normand, K. Raghavachari, A. Rendell, J. C. Burant, S. S. Iyengar, J. Tomasi, M. Cossi, N. Rega, J. M. Millam, M. Klene, J. E. Knox, J. B. Cross, V. Bakken, C. Adamo, J. Jaramillo, R. Gomperts, R. E. Stratmann, O. Yazyev, A. J. Austin, R. Cammi, C. Pomelli, J. W. Ochterski, R. L. Martin, K. Morokuma, V. G. Zakrzewski, G. A. Voth, P. Salvador, J. J. Dannenberg, S. Dapprich, A. D. Daniels, O. Farkas, J. B. Foresman, J. V. Ortiz, J. Cioslowski, and D. J. Fox, Gaussian, Inc., Wallingford CT, 2009.

[S2] A. D. Becke, *J. Chem. Phys.* **1993**, *98*, 1372.

[S3] C. Lee, W. Yang, R. G. Parr, *Phys. Rev. B* **1988**, *37*, 785.